# *Studying the Phase Diagram of QCD Matter at RHIC*

**A STAR white paper summarizing the current understanding and describing future plans**

**01 June 2014**

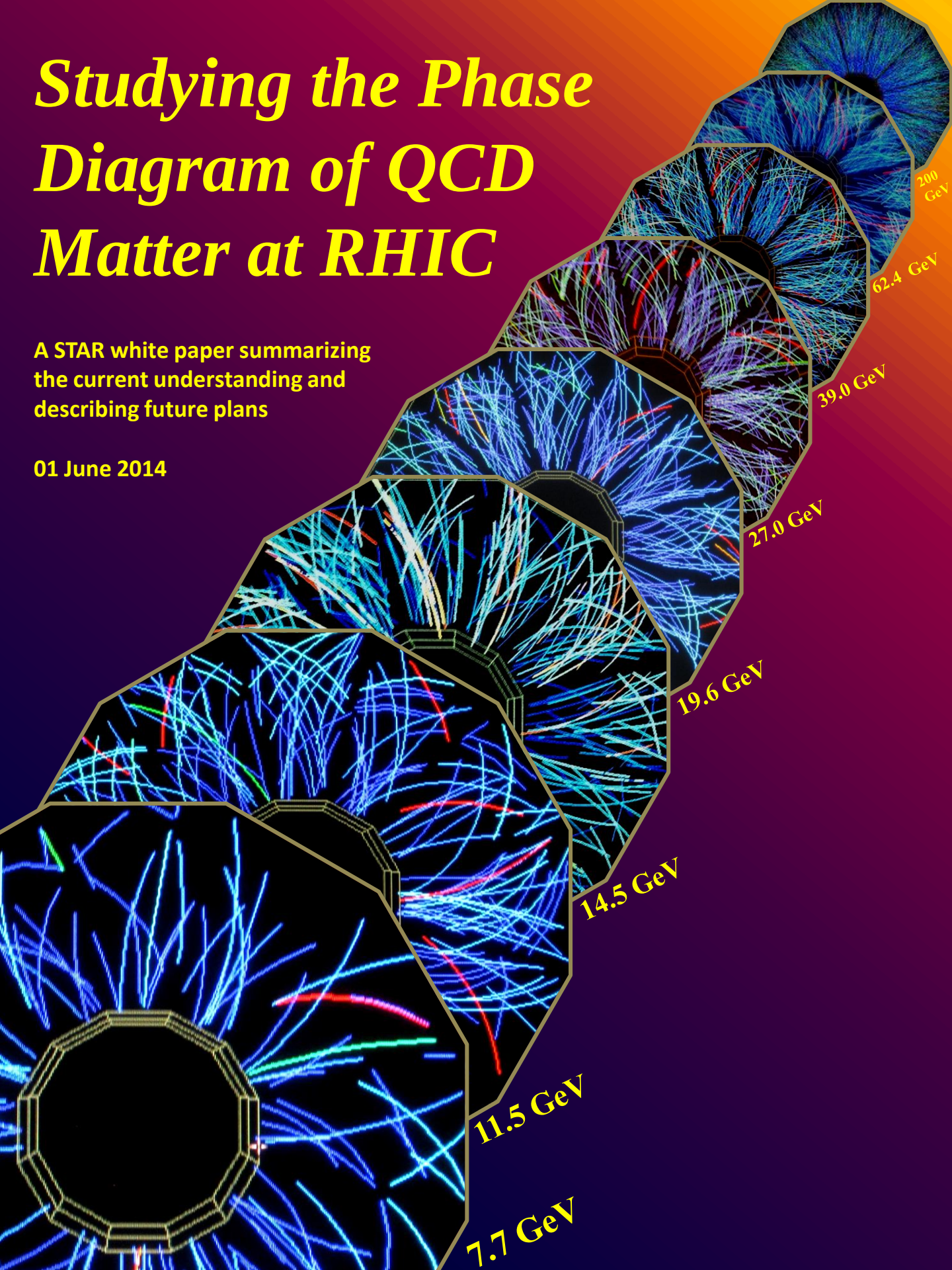

## Contents

**1 Introduction** **3**

**2 Review of BES-I Results and Theory Status** **5**
2.1 Region of the Phase Diagram Accessed in BES-I . . . . . 5
2.2 Search for the Critical Point . . . . . 8
2.3 Search for the First-order Phase Transition . . . . . 10
2.3.1 Directed Flow ($v_1$) . . . . . 10
2.3.2 Average Transverse Mass . . . . . 12
2.4 Search for the Threshold of QGP Formation . . . . . 13
2.4.1 Elliptic Flow . . . . . 13
2.4.2 Nuclear Modification Factor . . . . . 18
2.4.3 Dynamical Charge Correlations . . . . . 21
2.4.4 Chiral Transition and Dileptons . . . . . 24
2.5 Summary of BES-I . . . . . 27

**3 Proposal for BES Phase-II** **30**
3.1 Physics Objectives and Specific Observables . . . . . 30
3.1.1 $R_{CP}$ of identified hadrons up to $p_T$ = 5 GeV/$c$ . . . . . 32
3.1.2 The $v_2$ of $\phi$ mesons and NCQ scaling for indentified particles . . . . . 33
3.1.3 Three-particle correlators related to CME/LPV . . . . . 34
3.1.4 The centrality dependence of the slope of $v_1(y)$ around midrapidity . 36
3.1.5 Proton-pair correlations . . . . . 38
3.1.6 Improved $\kappa\sigma^2$ for net-protons . . . . . 40
3.1.7 Dilepton production . . . . . 41
3.2 Beam request . . . . . 43
3.3 The Fixed-Target Program . . . . . 45
3.4 The Importance of $p$+$p$ and $p$+A Systems . . . . . 45
3.5 Collider Performance . . . . . 47
3.6 Detector Upgrades . . . . . 47
3.6.1 *iTPC* . . . . . 48
3.6.2 *EPD* . . . . . 49

**4 Summary** **50**

## Executive Summary

The STAR Collaboration proposes a second phase of the Beam Energy Scan program at RHIC (BES Phase-II) to answer compelling questions about the phase structure of QCD matter that cannot be addressed using existing measurements. We propose dedicated low-energy running in 2018 and 2019 to take full advantage of accelerator and detector upgrades and focus on precision measurements in a targeted region identified in BES Phase-I.

- The first phase of the Beam Energy Scan program (BES-I) plus the top energy at RHIC has allowed access to a region of the QCD phase diagram covering a range of baryon chemical potential ($\mu_B$) from 20 to 420 MeV corresponding to Au+Au collision energies from $\sqrt{s_{NN}}$ = 200 to 7.7 GeV, respectively. Results from BES-I have further confirmed the evidence for the quark-gluon plasma (QGP) discovery at the top RHIC energy $\sqrt{s_{NN}}$ = 200 GeV. The results of the search for the critical point and the first-order phase boundary have narrowed the region of interest to collision energies below $\sqrt{s_{NN}}$ = 20 GeV. Current lattice QCD calculations suggest that key features of the phase diagram like the critical point and the first-order phase transition lie within the $\mu_B$ reach of the RHIC BES Phase-II program.
- The BES-I program has provided new information with measurements made at varying baryon density (e.g. azimuthal anisotropy of produced particles and dilepton invariant mass distributions). The lowest beam energies in the BES-I are expected to correspond to the highest compression of baryonic matter. Further, several measurements in BES-I coherently indicate that the role of partonic (hadronic) interactions increases (decreases) with beam energy.
- The proposed upgrades to the collider will increase the luminosity for future low energy runs by a factor of four to fifteen, depending on beam energy. The upgrades to the STAR detector system will significantly improve the quality of the measurements. The BES Phase-II program, with these upgrades, will allow for high-statistics measurements, with an extended kinematic range in rapidity and transverse momentum, using sensitive observables, to reveal the structure of the QCD phase diagram.

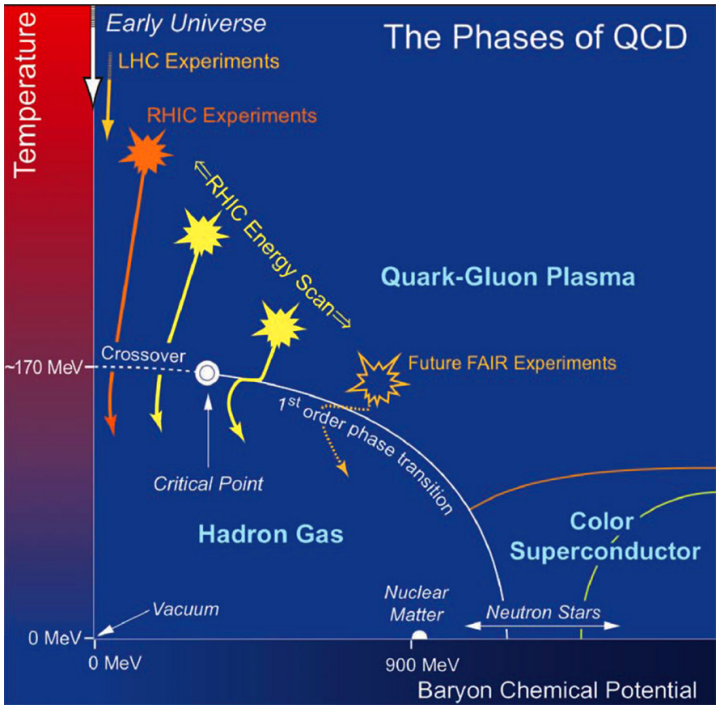


**Figure 1.** A conjectured QCD phase diagram with boundaries that define various states of QCD matter.

## 1. Introduction

A major goal of high-energy nuclear collisions is to determine the phase diagram for matter that interacts via the strong nuclear force. In contrast to the countless, very distinct phase diagrams found in condensed matter physics, the phase diagram probed in heavy-ion collisions is a unique and fundamental feature of Quantum Chromodynamics (QCD). The most experimentally accessible way to characterize the QCD phase diagram [1] is in the plane of temperature ($T$) and the baryon chemical potential ($\mu_B$) [2]. Figure 1 is a conjectured version with $\mu_B$ on the horizontal axis. It shows a schematic layout of the phases, along with hypothesized indications of the regions crossed in the early stages of nuclear collisions at various beam energies.

Hadronic matter is a state in which the fundamental constituents, quarks and gluons, are confined in composite particles, namely baryons and mesons. At high energy densities, QCD predicts a phase transition from a hadronic gas (HG) to a state of deconfined, partonic matter called the quark-gluon plasma (QGP) [3, 4]. In hot and dense QCD matter, the hadrons are melted into their constituent quarks, and the strong interaction becomes the dominant feature of the physics. In addition to the confined-deconfined transition, a chiral phase transition is postulated. Since the intrinsic scale of QCD is $\Lambda_{\rm QCD} \sim 200$ MeV, it is conceivable that the chiral phase transition line extends from around $T \sim \Lambda_{\rm QCD}$ at low baryon number density ($n_B$) to around $n_B \sim \Lambda_{\rm QCD}^3 \sim 1/{\rm fm}^{-3}$ at low $T$.

Lattice QCD calculations have established that the quark-hadron transition to be a crossover transition at the temperature around 154 MeV for $\mu_B = 0$ [5, 6, 7, 8, 9]. On the

other hand, QCD-based models predict a first-order phase transition and the existence of an end point or critical point at high $\mu_B$ [10, 11]. However, the locations of the phase boundary and the critical point in this framework depend on model assumptions [12]. Experimentally, laboratory studies of relativistic heavy-ion collisions can provide us only with a chance to make microscopic, short-lived volumes of QCD matter. We access properties of the matter by studying the evolution of these systems as they expand, cool, and possibly undergo phase transitions. Experiments at the Relativistic Heavy Ion Collider (RHIC) and the Large Hadron Collider (LHC) have provided compelling evidence of the formation of a deconfined state of quarks and gluons (QGP) for matter close to $\mu_B = 0$. The existence of a critical point and first-order phase transition at higher $\mu_B$ remains to be confirmed experimentally.

In order to study experimentally the QCD phase structure as a function of $T$ and $\mu_B$, a scan over beam energies is employed. Several collision energies are used to create systems which form at a variety of initial coordinates in $T$ and $\mu_B$. As the systems evolve, the adiabatic expansion is governed by the QGP equation of state. Therefore, as the system expands, $T$ is reduced and $\mu_B$, which is a measure of the excess of quarks relative to antiquarks, may also evolve. The excess of quarks is due to the valence quarks of the stopped participant baryons from the two colliding nuclei. By creating systems with a broad range of initial conditions, it is hoped that the different reaction trajectories cross the phase boundary at different $T$ and $\mu_B$ values and that this allows us to access interesting features in the phase diagram (i.e. critical point and first-order phase transition). Heavy-ion collision programs at the Alternating Gradient Synchrotron (AGS) and the Super Proton Synchrotron (SPS) launched the study of some of the physics topics targeted by the RHIC BES. For example, the onset of deconfinement has been claimed at the SPS [13]. Although the fixed-target experiments benefited from relatively high collision rates, analyses of data from these early programs are complicated, as the experimental acceptances and particle identification vary with beam energy. Neither program could reach the high beam energies where the QGP is cleanly established. Phase-I of a Beam Energy Scan (BES-I) program at RHIC was not subject to these limitations and began taking data in the year 2010 [14, 15].

The purpose of the BES-I program was three-fold: (a) to search for threshold energies for the QGP signatures that have already been established at the top RHIC energies, thereby corroborating the past QGP discoveries; (b) to search for signatures of a first-order phase transition; and (c) to search for a QGP/HG critical point. Data were collected during 2010 and 2011 at 6 energies. Data from a final BES-I energy point at 14.5 GeV were collected in February and March of 2014. The details of the BES-I program are listed in Table 1.

Here we report a summary of selected experimental results from BES-I. During the course of the presentation of results, we also discuss the current status of theory. For some of the results from BES-I, as discussed below (Section 2), the strength of the conclusions is limited by the uncertainty in the measurements. More definitive conclusions will be possible after a second phase of the program (BES Phase-II). In this second phase, we propose to concentrate on collecting high event statistics at the lower-energy end of the BES-I range ($\sqrt{s_{NN}} < 20$ GeV). Details of the BES Phase-II proposal will be discussed in Section 3. In that section, we also comment on the possibility of an increase in luminosity for the lower

**Table 1.** An overview of Beam Energy Scan Phase-I. The $\mu_B$ values are estimated from the systematics of central collisions in Ref. [19]. The 200 GeV is also listed in the table as a reference.

| Beam Energy (in GeV) | Baryon Chemical Potential (in MeV) | Year of Data Taking | Event Statistics (Millions) | Beam Time (Weeks) |
|---|---|---|---|---|
| 200 | 20 | 2010 | 350 | 11 |
| 62.4 | 70 | 2010 | 67 | 1.5 |
| 39 | 115 | 2010 | 130 | 2.0 |
| 27 | 155 | 2011 | 70 | 1.0 |
| 19.6 | 205 | 2011 | 36 | 1.5 |
| 14.5 | 260 | 2014 | 20 | 3.0 |
| 11.5 | 315 | 2010 | 12 | 2.0 |
| 7.7 | 420 | 2010 | 4 | 4.0 |

beam energies through electron cooling at RHIC, and briefly discuss our proposed detector upgrades to enhance the scientific/technical quality of the various results. Finally, in Section 4, we summarize the scientific part of the RHIC BES program.

## 2. Review of BES-I Results and Theory Status

### *2.1. Region of the Phase Diagram Accessed in BES-I*

Experimentally, different regions of the phase diagram are accessed by changing the beam energy. Both initial $T$ and $\mu_B$ vary as functions of the center-of-mass energy ($\sqrt{s_{NN}}$) [16]. This is the strategy adopted in the BES program at RHIC [14, 15]. It is possible to estimate the $T$ and $\mu_B$ regions of the phase diagram accessed for a given collision energy through the study of the hadron spectra. These spectra reflect the properties of the bulk matter at kinetic freeze-out, after elastic collisions among the hadrons have ceased. Information on the earlier stages can be deduced from the integrated yields of the different hadron species, which change only via inelastic collisions. The point in time at which these inelastic collisions cease is referred to as chemical freeze-out, which takes place before kinetic freeze-out. In the BES-I program at RHIC, almost all species of hadrons in the light and strange quark sectors, including $\pi^{\pm}$, $K^{\pm}(K^0_S)$, $p(\bar{p})$, $\phi$, $\Lambda$, $\Xi$, and $\Omega$ have been detected and yields were measured as a function of collision centrality. As an example, Fig. 2 shows a representative plot of the invariant yields of $\pi^+$, $K^+$, $K^0_S$, $\phi$, $p$, $\Lambda$ and $\Xi^-$ as a function of $m_T$ - $m$, where $m_T = \sqrt{m^2 + p_T^2}$ is the transverse mass, $m$ is the rest mass of the hadron and $p_T$ the transverse momentum. The results are shown for various collision centralities in Au+Au collisions at $\sqrt{s_{NN}}$ = 11.5 GeV.

Within a statistical model which assumes thermodynamic equilibrium, the particle yields at chemical freeze-out in a system of volume $V$ can be given by

$$N_i/V = \frac{g_i}{(2\pi)^3}\gamma_S^{S_i}\int \frac{1}{\exp\left(\frac{E_i-\mu_B B_i-\mu_S S_i}{T_{ch}}\right)\pm 1} d^3p\,, \tag{1}$$

where $N_i$ is the abundance of particle species $i$, $g_i$ is the spin degeneracy, $B_i$ and $S_i$ are the baryon number and strangeness number, respectively, $E_i$ is the particle energy, and the integral

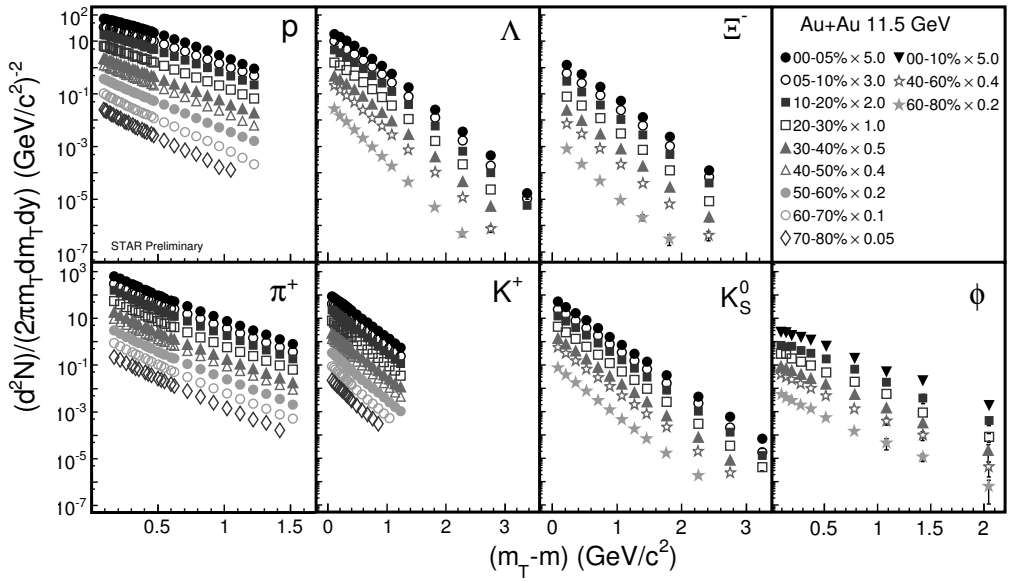


**Figure 2.** Invariant yields versus $m_T$ - $m$ of hadrons produced in Au+Au collisions at various collision centralities at $\sqrt{s_{NN}}$ = 11.5 GeV.

is taken over all momentum space [17]. The model parameters are the chemical freeze-out temperature ($T_{ch}$), the baryon ($\mu_B$) and strangeness ($\mu_S$) chemical potentials, and the *ad hoc* strangeness suppression factor ($\gamma_S$). Measured particle yields (obtained by integrating the distributions in Fig. 2 over $p_T$) have been used to estimate the values of $T_{ch}$ and $\mu_B$ at chemical freeze-out, see Figure 3(a), using the statistical model THERMUS [18] and assuming that the system can be represented by a Grand Canonical ensemble.

The figure shows that RHIC programs, the top energy plus the BES-I, cover the $\mu_B$ region from $\sim$ 20 MeV ($\sqrt{s_{NN}}$ = 200 GeV) to $\sim$ 420 MeV ($\sqrt{s_{NN}}$ = 7.7 GeV), which is a larger range than at any other heavy-ion facility. The yellow band shows empirical $T_{ch}$ versus $\mu_B$ trends based on data obtained prior to the BES-I program using statistical models in the literature [19, 21].

The graph in Fig. 3(a) shows only a single point at chemical freeze-out in the system's expansion trajectory in the $T$ vs. $\mu_B$ plane. The starting point of each trajectory is governed by the primordial conditions prevailing during the early equilibration phase. The evolution of the system is then influenced by the equation-of-state (EOS) as the system expands and cools until it reaches chemical freeze-out. In addition, the BES-I program provided measurements of the centrality dependence of the freeze-out parameters [22, 23]. Measurements of the centrality dependence have not previously been available in heavy-ion collisions and could be used to constrain the expansion dynamics. In BES Phase-II, a systematic measurement of the yields of a variety of produced hadrons versus rapidity, centrality, and beam energy will address questions about the evolution of the hadron yields between the initial hadronization and the final thermal equilibrium [24] and about the possibility of successive hadronization [25]. This

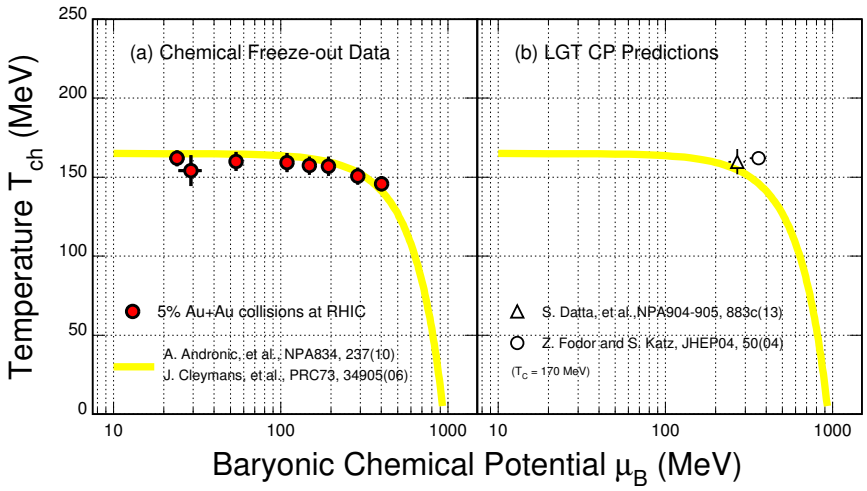


**Figure 3.** (a) Chemical freeze-out temperature ($T_{ch}$) versus baryonic chemical potential ($\mu_B$) obtained from a statistical model [20, 19] fit to yields of hadrons produced in 0-5% central Au+Au collisions at RHIC. The yellow bands are the empirical results from fitting experimental data acquired prior to the BES-I program by a statistical model. (b) The positions of the QCD critical point from two different lattice gauge theory calculations in the $T_{ch}$ versus $\mu_B$ plane are shown.

could lead to further development, understanding, and refinement of the statistical models. Recently, the possibility of extracting freeze-out properties by comparing the higher moments of multiplicity distributions of conserved numbers (net-charge and net-baryons) to QCD calculations of high order susceptibilities on the lattice has been proposed [26, 27]. This has been possible due to the construction of proper observables that allow for comparison between experiment and QCD calculations [28, 29].

Two estimates of the QCD critical point from lattice gauge theory calculations [30, 31] in the $T-\mu_B$ plane taking $T_c$ = 170 MeV are shown in Fig. 3(b). Based on these current estimates of the critical point from QCD calculations, we observe that the RHIC BES-I program scanned from energies for which the matter expands and cools through a crossover transition down to those which could contain key features of the phase diagram of QCD matter; specifically, the detailed study of the energy range from 7.7 to 19.6 GeV proposed in BES Phase-II is well suited to identify the critical point and the first-order phase transition boundary.

The transverse momentum distributions of the different particles contain two components, one random and one collective. The random component can be identified as the one that depends on the temperature of the system at kinetic freeze-out ($T_{kin}$). The collective component, which arises from the matter density gradient from the center to the boundary of the fireball created in high-energy nuclear collisions, is generated by collective flow in the transverse direction and is characterized by its velocity ($\langle\beta\rangle$), also called the radial flow. Assuming that the system attains thermal equilibrium, the blast-wave formulation [32] can be used to extract $T_{kin}$ and $\langle\beta\rangle$. The $T_{kin}$ versus $\langle\beta\rangle$ values obtained from the simultaneous

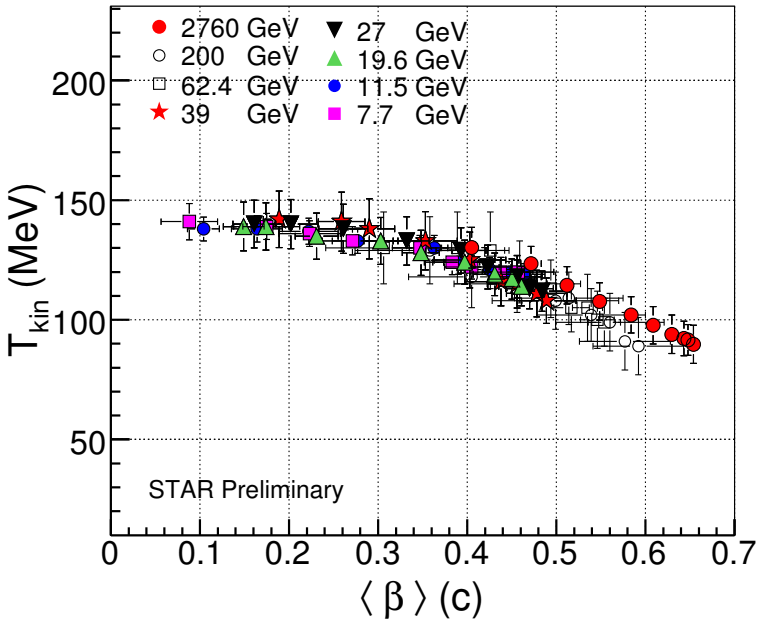


**Figure 4.** Kinetic freeze-out temperature ($T_{kin}$) versus the average collective flow in the transverse direction ($\langle\beta\rangle$) in high energy heavy-ion collisions for different collision centralities. At each collision energy, the data points with lower $\langle\beta\rangle$ values correspond to peripheral collisions and those with the larger $\langle\beta\rangle$ values correspond to central collisions.

fits to the $m_T - m$ distributions of $\pi$, $K$, and $p$ (as shown in the representative plot in Fig. 2) at midrapidity at RHIC for various collision energies are shown in Fig. 4. Also shown are the corresponding results from Pb+Pb collisions at $\sqrt{s_{NN}}$ = 2.76 TeV from ALICE at the LHC [33]. The $T_{kin}$ values in central collisions are lower than the corresponding values for $T_{ch}$ (shown in Fig. 3) although the difference decreases at lower beam energies. At all the beam energies studied (BES-I, 200 GeV, and LHC [33]), there is an anti-correlation between $T_{kin}$ and $\langle\beta\rangle$. This shows that peripheral collisions have a higher value of temperature (freeze-out earlier) and less collectivity is developed compared to central collisions (freeze-out later) [34].

### *2.2. Search for the Critical Point*

Thermodynamic principles suggest that there should be a critical point in QCD matter where the first-order phase transition ends and the transition becomes a crossover [5, 9], at which point the phase boundaries effectively cease to exist. The characteristic experimental signature of the QCD critical point is large fluctuations in event-by-event multiplicity distributions of conserved quantities like net-charge, net-baryon number, and net-strangeness. The variances of these distributions, $\langle(\delta N)^2\rangle$, are proportional to the square of the correlation length ($\xi$). It has been shown that higher moments ($\langle(\delta N)^3\rangle \sim \xi^{4.5}$ and $\langle(\delta N)^4\rangle \sim \xi^7$) have stronger dependences on $\xi$ than the variance and might have higher sensitivity [35, 36, 37]. In addition,

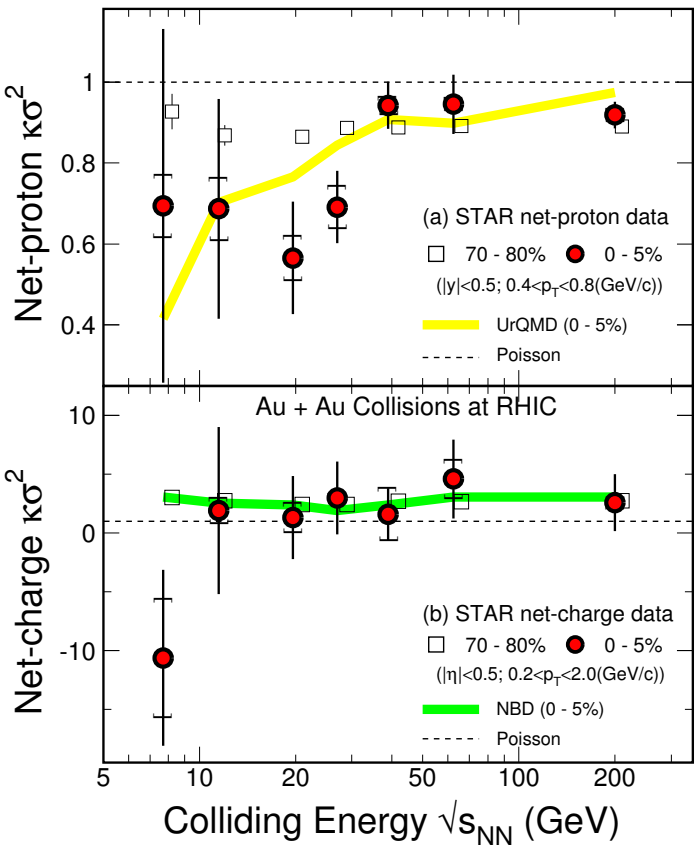


**Figure 5.** Collision energy dependence of net-proton (top panel) [40] and net-charge (bottom panel) [42] $\kappa\sigma^2$ from Au+Au collisions at RHIC. The red solid circles correspond to 0-5% central collisions and the open squares represent 70-80% peripheral collisions. The vertical error bars are statistical and the caps correspond to systematic errors. The yellow solid band in the top panel represents 0-5% central Au+Au collision results from UrQMD simulations and the green solid band in the bottom panel is the result where proton and anti-proton distributions follow independent negative binomial statistics. The dashed line in each panel represents the expectation from proton and anti-proton distributions following Poisson statistics.

the moments are related to the susceptibilities ($\chi$) [38] and hence a comparison can be directly made to QCD calculations [28, 29]. Motivated by these considerations, STAR has studied the kurtosis times the variance ($\kappa\sigma^2$) of net-proton (a proxy for net-baryon) and net-charge distributions to search for the critical point [39, 40]. In the absence of a critical point, the hadron resonance gas model [41] suggests that the $\kappa\sigma^2$ values will be close to unity and have a monotonic dependence on $\sqrt{s_{NN}}$ [43]. However, because $\kappa\sigma^2$ is related to the ratio of conserved number susceptibilities in QCD models ($\kappa\sigma^2 = \frac{\chi^{(4)}}{\chi^{(2)}/T^2}$ [28]), it is expected to show a non-monotonic dependence on $\sqrt{s_{NN}}$ close to the critical point.

Figure 5 shows the $\kappa\sigma^2$ for net-proton (top panel) [40] and net-charge (bottom panel) [42] distributions in Au+Au collisions at midrapidity as a function of colliding energy for two different collision centralities (0-5% and 70-80%). The net-proton $\kappa\sigma^2$ values for the 0-5% centrality selection at $\sqrt{s_{NN}}$ = 19.6 and 27 GeV are observed to deviate from: (a) the values from 70-80% peripheral collisions which are expected to create small systems which are dominated by two-to-two processes and do not show significant bulk properties; (b) Poisson and hadron resonance gas expectation values, which would correspond to uncorrelated emission and are close to unity; and (c) transport-model-based UrQMD [44, 45] calculations, which represent the expectations of expanding drops of finite hadronic matter which does not experience a phase transition. A fourth baseline based on the model of independent production is under investigation and was briefly discussed in [40]. The conclusions which can be drawn from the net-charge $\kappa\sigma^2$ values are not clear because of the large uncertainties, which are driven by the larger value of the $\sigma$ for the net-charge distributions. In addition, finite acceptance measurements of net-charge fluctuations are subject to the effect of resonance decay. Within the current statistical uncertainties, the data do not show a non-monotonic variation of the $\kappa\sigma^2$ of net-charge distributions as a function of $\sqrt{s_{NN}}$. A possible non-monotonic variation of the $\kappa\sigma^2$ of the net-proton distribution is not excluded by the existing STAR data. High event statistics for collisions below 20 GeV in BES Phase-II will help clarify these issues.

### *2.3. Search for the First-order Phase Transition*

A first-order phase transition is characterized by a discontinuity in one of the state variables. Lattice QCD predicts that there should be a discontinuity in the density below $T_C$ [46]. A first-order phase transition is also characterized by an unstable coexistence region. This spinodal region will exhibit a change in compressibility, i.e. a softening of the EOS. A signature of this softening of the EOS is the pattern of directed flow (like its slope at midrapidity) versus beam energy [47, 48, 49]. Such flow patterns can be obtained by studying the Fourier expansion of the azimuthal angle ($\phi$) distribution of produced particles with respect to the reaction plane angle ($\Psi_R$) [50]. Directed flow can be quantified by the first Fourier coefficient ($v_1$), while the elliptic flow is given by the second coefficient ($v_2$).

Another possible signature is a saturation of the average transverse momentum as a function of collision energy. It is based on the relation of temperature and entropy to the average transverse momentum and multiplicity, respectively. This signature was originally proposed by Van Hove in the context of proton-proton collisions [51]. It was argued that a plateau in the average transverse momentum beyond a certain value of multiplicity will indicate the onset of the formation of a mixed phase of QGP and hadrons, analogous to the plateau observed in the variation of temperature with entropy in a first-order phase transition scenario.

*2.3.1. Directed Flow ($v_1$)* Hydrodynamic calculations [47, 48, 49], including a three-fluid hydrodynamic model [48, 49] whose EOS incorporates a first-order phase transition, suggest

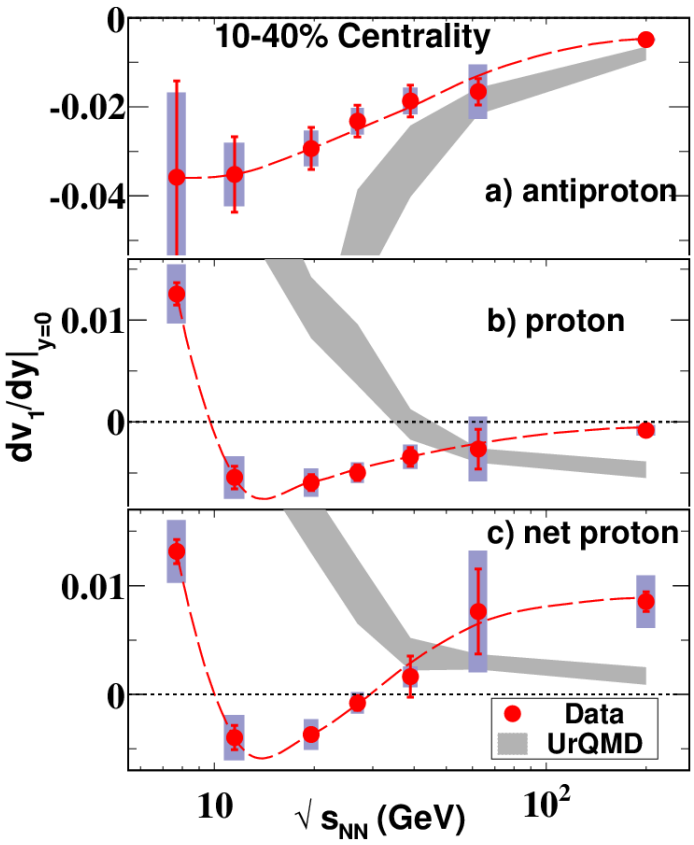


**Figure 6.** Directed flow slope ($dv_1/dy$) near mid-rapidity as a function of beam energy for intermediate-centrality (10-40%) Au+Au collisions. Panels (a), (b), and (c) report STAR's measurement for antiprotons, protons, and net-protons, respectively, along with corresponding calculations from the UrQMD hadronic transport model [44, 45] subject to the same cuts and fit conditions. The systematic uncertainties on the measurements are shown as shaded bars. The dashed curves are a smooth fit to guide the eye.

that the $v_1$ of net-baryons is sensitive to the early collision dynamics and can be used as a signature for the first-order phase transition. These calculations predict a non-monotonic variation of directed flow slope of baryons (or net-baryons) around midrapidity as a function of beam energy and feature a prominent minimum around $\sqrt{s_{NN}}$ = 4 GeV and a double sign change in the $v_1$ slope, which is not seen in the same hydrodynamic model without a first-order phase transition. More up-to-date hydrodynamic calculations [52, 53] confirm this earlier prediction, but yield consistently larger $v_1$ magnitudes than observed by STAR in BES-I.

Figure 6(a) and (b) shows the beam energy dependence of the slope of directed flow at midrapidity ($dv_1/dy$) for antiprotons and protons, respectively [54]. For intermediate-centrality (10-40%) collisions, the proton slope decreases with energy and changes sign from positive to negative between 7.7 and 11.5 GeV, shows a minimum below 19.6 GeV, and remains small and negative up to 200 GeV. In contrast, the corresponding antiproton results always remain negative and approach the proton results at high beam energies. For

comparison, the UrQMD hadronic transport model [44, 45], which has no phase transition mechanism, does not show a non-monotonic behavior in the same energy range as the data. Recent hybrid [53] and Parton-Hadron-String Dynamics [55] calculations do not show a minimum in proton $v_1$.

The energy dependence of proton $dv_1/dy$ involves an interplay between the proton $v_1$ associated with the baryon number transported from the initial state to mid-rapidities, and the proton $v_1$ from pair production near mid-rapidity. The importance of the second mechanism increases strongly with beam energy. A way to distinguish between the two mechanisms would be informative. We define the slope, $[dv_1/dy]_{\text{net-}p}$, based on expressing the rapidity dependence of directed flow for all protons as

$$[v_1(y)]_p = r(y)[v_1(y)]_{\bar{p}} + [1 - r(y)]\,[v_1(y)]_{\text{net-}p}\,,$$

where $r(y)$ is the observed rapidity dependence of the ratio of antiprotons to protons at each beam energy [54]. For reasons set out in Ref. [54], it is assumed that the antiproton directed flow is a proxy for the directed flow of produced protons. Therefore, $[dv_1/dy]_{\text{net-}p}$ isolates, as far as possible, the contributions from transported initial-state baryonic matter. Figure 6(c) shows that the $v_1(y)$ slope for net protons is negligibly different from protons below 19.6 GeV, but then rises, crosses zero between 27 GeV and 39 GeV, and remains positive up to 200 GeV. The UrQMD model [44, 45] shows a monotonic trend, with a positive slope at all energies.

An interpretation of the changing sign of the $v_1$ slope is that it reflects a change in EOS. At a given energy where the system undergoes a first-order parton-hadron phase transition, one expects the formation of a mixed phase, where the pressure gradient is small. The softest pressure could produce the observed minimum in the proton $v_1$ slope parameter. At higher energies, pair production is dominant at mid-rapidity and transported baryons have a relatively small influence. As there is no preferred direction for pair-produced hadrons, the slope parameter approaches zero. At lower beam energies, baryon transport is dominant, hence the slope parameter is positive. A mean-field model study shows that the energy-dependent baryon potential plays an important role in this region [56]. In the search for a first-order phase transition in the QCD phase diagram, the findings from the $dv_1/dy$ analysis from the STAR BES-I strongly motivate further measurements at $\sqrt{s_{NN}} < 20$ GeV where the softest region of the EOS is suggested. To better understand the possible role and relevance of stopping in the existing data on proton and net-proton directed flow, new higher-statistics $v_1$ measurements as a function of centrality are needed.

*2.3.2. Average Transverse Mass* Figure 7 (left panel) shows $\langle m_T \rangle - m$ for $\pi$ and $K$ in central Au+Au collisions as a function of the center-of-mass energy at RHIC [17]. The $\langle m_T \rangle - m$ can be interpreted as a measure of thermal excitation in the transverse direction (temperature), while $dN/dy$, which is a measure of the entropy ($S$), has been shown to be proportional to $\ln(\sqrt{s_{NN}})$. Also shown in Fig. 7 are results from Au+Au collisions at the AGS [57, 58, 59, 60, 61, 62], from Pb+Pb collisions at the SPS [63, 13] and LHC [33]. The $\langle m_T \rangle - m$ values increase with $\sqrt{s_{NN}}$ at AGS energies, stay independent of $\sqrt{s_{NN}}$ at SPS and RHIC BES-I energies, and then tend to rise again with increasing $\sqrt{s_{NN}}$ at the higher

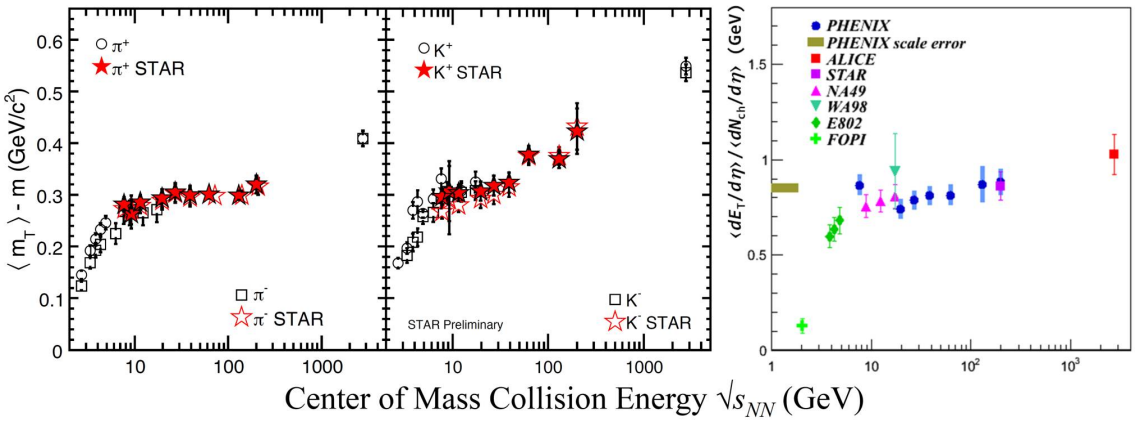


**Figure 7.** Left panels: Center-of-mass energy dependence of $\langle m_T \rangle - m$ of $\pi$ and $K$, in central Au+Au collisions at midrapidity at RHIC. Also shown are the corresponding results from experiments at the AGS [57, 58, 59, 60, 61, 62], SPS [63, 13], and LHC [33]. The errors shown are the quadrature sum of statistical and systematic uncertainties. Right panel: The average transverse energy, scaled by the charged particle multiplicity at mid-rapidity, as a function of collision energy observed by the PHENIX, ALICE, STAR, NA49, WA98, E802, and FOPI Collaborations [64].

beam energies at RHIC [17] and at the LHC [33]. The results shown in the figure reflect the characteristic signature of a first-order phase transition, as first proposed by Van Hove [51].

For comparison to STAR's $\langle m_T \rangle - m$, we show a compilation of $\langle dE_T/d\eta \rangle / \langle dN_{ch}/d\eta \rangle$ results prepared by the PHENIX collaboration [64] in Fig. 7 (right panel). As one can see in the figure, there is qualitative agreement between the saturation in $\langle E_T \rangle$ (right panel) and $\langle m_T \rangle - m$ (left panel), although the absolute values of $\langle E_T \rangle$ are much larger.

### *2.4. Search for the Threshold of QGP Formation*

Several distinct signatures of the formation of a new state of hot and dense matter, where relevant degrees of freedom are quarks and gluons, have been reported on the basis of data from top RHIC energy [34, 65, 66]. These include (i) the measurement of a large magnitude of the elliptic flow (close to that expected from ideal hydrodynamics in a system of deconfined quarks and gluons) for both light and strange-quark carrying hadrons, and the discovery of the number-of-constituent-quark ($n_Q$) scaling of elliptic flow of identified hadrons [67, 68, 69, 70]; (ii) the observation of the phenomenon of jet quenching through the measurement of the nuclear modification factor of produced hadrons at high transverse momentum [71, 72, 73, 74]; and (iii) the observation of dynamical charge correlations with respect to the reaction plane [75, 76]. In this section, we discuss how the BES-I results corroborate the findings of the formation of QGP at the top RHIC energy.

*2.4.1. Elliptic Flow* The study of collective flow in relativistic nuclear collisions could provide insights into the EOS of the matter created during heavy-ion collisions. As discussed

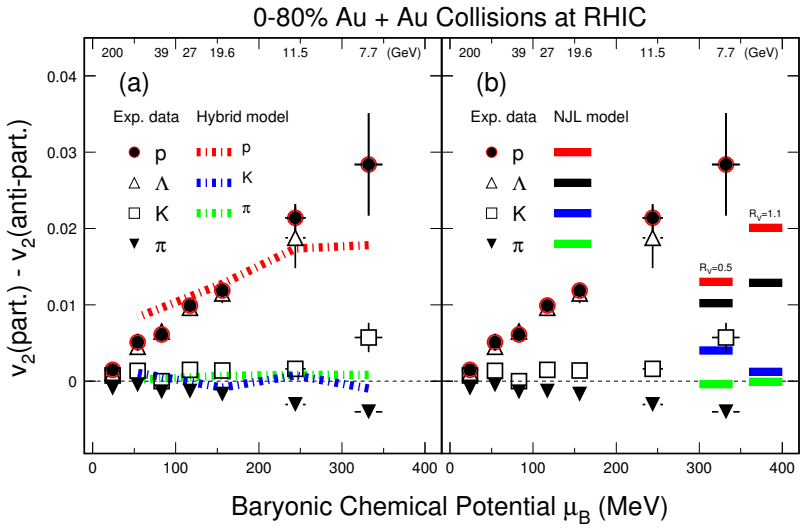


**Figure 8.** The measured difference in integrated $v_2$ between particles and their corresponding antiparticles: pions (filled triangles), kaons (open squares), Λs (open triangles), and protons (filled circles), all shown as a function of baryonic chemical potential and collision energy for 0–80% Au+Au collisions [83, 84]. Only statistical error bars are shown. Panels (a) and (b) show the comparison with model calculations from Refs. [86] and [87, 88], respectively.

earlier, there are two types of azimuthal anisotropy that are commonly studied in heavy-ion collisions, directed flow ($v_1$) and elliptic flow ($v_2$). In this subsection, we concentrate on $v_2$. The $v_2$ coefficient has proven to be one of the most discussed probes of the dynamics in Au+Au collisions at RHIC [77, 78, 79, 80, 81].

Figure 8 shows the first experimental observation of the difference in the integrated $v_2$ at midrapidity between particles and their corresponding antiparticles for pions, kaons, Λs, and protons, shown as a function of the baryonic chemical potential [82] and center-of-mass energy for minimum-bias (0–80%) Au+Au collisions [83, 84]. The $v_2$ difference is positive for all the hadrons studied, except for pions. The difference in $v_2$ is almost linearly proportional to the value of the baryon chemical potential. This indicates a connection between the $v_2$ differences and the net-baryon density at chemical freeze-out.

The negative value of the $v_2$ difference for pions has been predicted [85] to be due to the interplay between the strong external magnetic field and the density wave of both electric and chiral charges, in semi-central high-energy nuclear collisions. On the other hand, several studies in the literature [86, 87, 88, 90] attempt to explain the observed differences with hadronic interactions at lower beam energies. In Fig. 8(a), dashed lines represent model results from a hybrid calculation featuring Boltzmann transport with an intermediate hydrodynamic stage [86]. This approach can reproduce the observed $v_2$ difference between baryons and antibaryons. It reproduces the small value of the $v_2$ difference for pions, however, the sign of the observable in the model is opposite to that of the observations. The authors of Ref. [86] have argued that the BES-I data show that it is important to properly treat strangeness

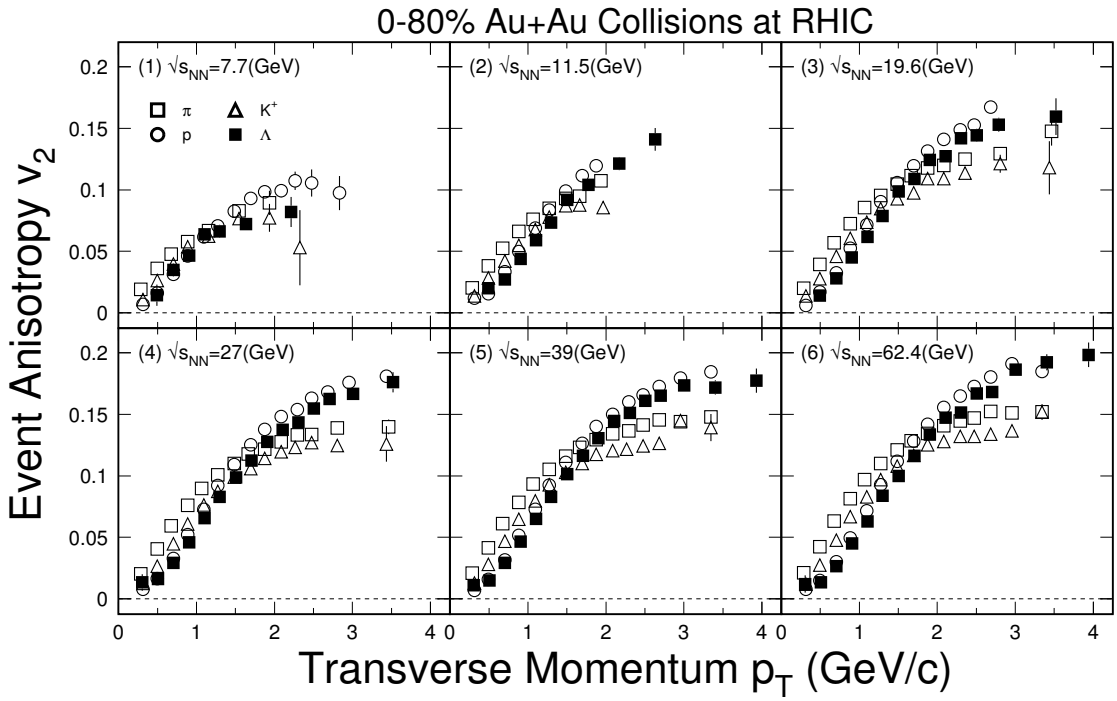


**Figure 9.** The experimental results of the identified hadron anisotropy parameter $v_2$ from minimum bias (0–80%) Au+Au collisions at six collision energies [83, 84].

production and isospin conservation.

Figure 8(b) shows the results from Nambu-Jona-Lasinio (NJL) mean-field model calculations with two values of the ratio ($R_v$) of the vector coupling to the scalar-pseudoscalar coupling [87, 88] that are compared to the data for $\sqrt{s_{NN}}$ = 7.7 GeV. The model reproduces the correct order of the $v_2$ splitting but misses the values of the $v_2$ differences quantitatively. The authors have pointed out that the magnitude of the $v_2$ splitting is sensitive to the vector coupling which, in turn, could be baryon-density dependent. Note that the vector coupling is close to zero at vanishing net-baryon density. According to Ref. [89], such baryon-density dependent vector interactions may affect the location of the critical point in the QCD phase diagram. The authors of Ref. [90] have pointed out the importance of the transport of baryon charge in high-energy nuclear collisions as a possible explanation of the experimental data.

Figure 9 shows the $v_2$ of identified hadrons ($\pi^+$, $K^+$, $p$, and $\Lambda$) as a function of transverse momentum for minimum-bias (0–80%) Au+Au collisions at RHIC BES-I energies [83, 84]. As was observed at the top RHIC energy, below a $p_T$ of 2 GeV/$c$, the $v_2(p_T)$ values are hadron-mass ordered. Lighter hadrons have a larger $v_2$ compared to heavier hadrons. Above $p_T$ = 2 GeV/$c$, the characteristic baryon-meson splitting of $v_2(p_T)$ is seen for $\sqrt{s_{NN}}$ = 27, 39, and 62.4 GeV collisions, as was observed at $\sqrt{s_{NN}}$ = 200 GeV [81]. Such a splitting was a basis of the claim of recombination being a process of hadronization [91, 92, 93], which in turn is connected to the existence of partonic collectivity, and the formation of a deconfined phase in high energy heavy-ion collisions. At $\sqrt{s_{NN}}$ = 19.6 GeV, the baryon-meson splitting appears

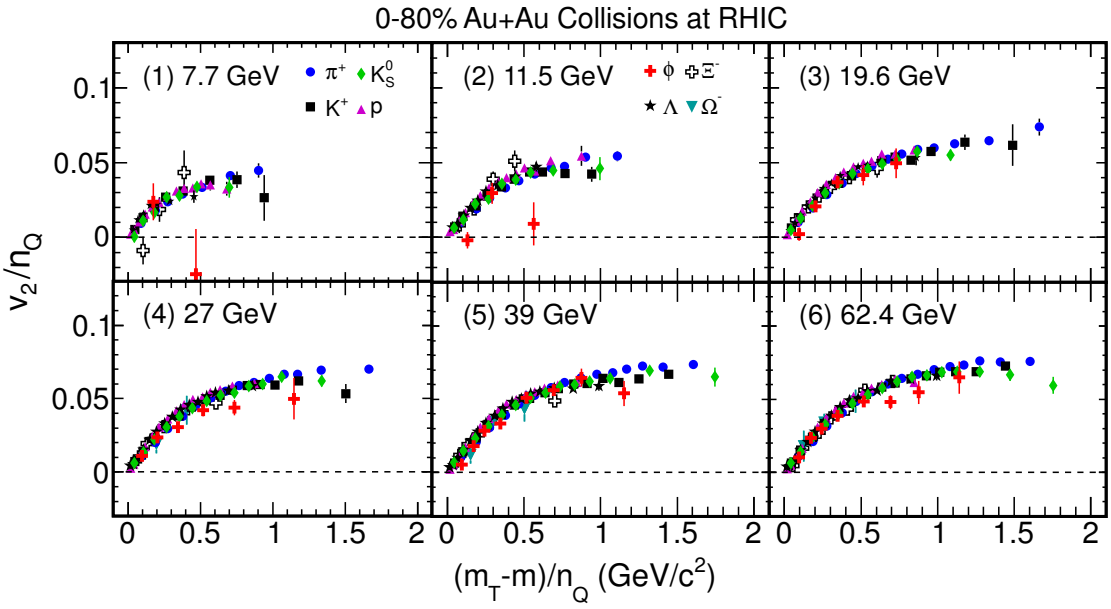


**Figure 10.** The number-of-constituent-quark scaled anisotropy parameter $v_2$, for identified hadrons from minimum-bias (0–80%) Au+Au collisions at six collision energies [83, 84]. Here $n_Q$ stands for the number of constituent quarks.

to be reduced, thereby suggesting a reduced contribution to the collectivity. The limited range of $p_T$ allowed by the event statistics at $\sqrt{s_{NN}}$ = 7.7 and 11.5 GeV makes conclusions difficult for these energies.

Figure 10 shows $v_2$ scaled by the number of constituent quarks ($n_Q$) for identified hadrons, as a function of $n_Q$-scaled $m_T - m$ for 0-80% Au+Au collisions at $\sqrt{s_{NN}}$ = 7.7, 11.5, 19.6, 27, 39, and 62.4 GeV [83, 84]. For the momentum range studied, the $n_Q$ scaling is observed to be within $\sim$ 10% for all the plotted beam energies [83, 84]. The major differences compared to the corresponding results at $\sqrt{s_{NN}}$ = 200 GeV are as follows. (i) At the top RHIC energy, all particles and antiparticles together follow the $n_Q$ scaling in $v_2$. This conclusion is confirmed by the PHENIX analysis of $v_2$ at 39 and 62.4 GeV [94]. However, from the observations in Fig. 8, it is clear that this is no longer the case at lower BES-I energies. The particles and antiparticles are observed to separately follow the $n_Q$ scaling in $v_2$ [83, 84]. (ii) At 7.7 and 11.5 GeV, the $v_2$ of the $\phi$ meson hints at being lower than that of the other hadrons (but much increased statistics are needed). The smaller $v_2$ values of the $\phi$ meson, which has a smaller hadronic interaction cross section, may indicate that hadronic interactions become more important than partonic effects for the systems formed at collision energies below 19.6 GeV [95, 96]. This aspect is discussed in further detail below. In addition, as suggested in Fig. 9, the baryon-meson splitting at intermediate $p_T$ is reduced at the lower collision energies, which is consistent with the findings that hadronic interactions at these energies dominate in the systems formed.

The study of the $v_2$ of particles with a very small hadronic cross section may elucidate the partonic dynamics and collectivity in heavy-ion collisions. The $\phi$ meson, which is a bound

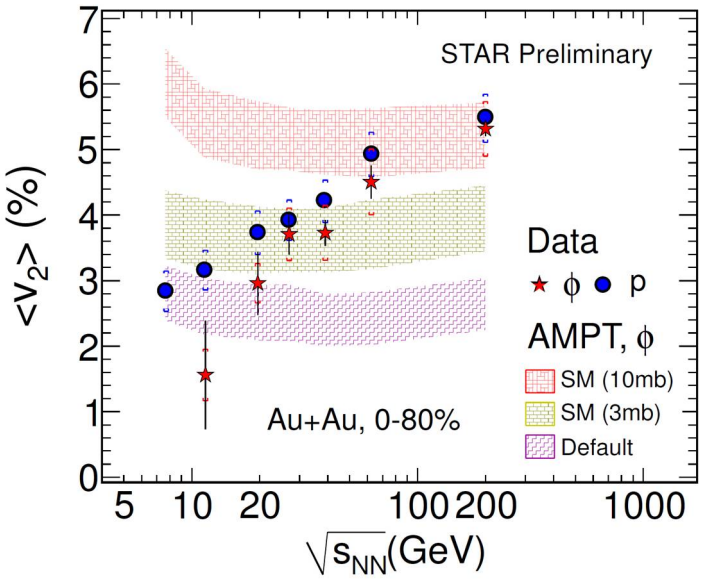


**Figure 11.** The $p_T$-integrated ϕ-meson and proton $v_2$ for Au+Au minimum-bias (0–80%) collisions at mid-rapidity ($| y |< 1.0$) at RHIC s a function of $\sqrt{s_{NN}}$. The ϕ meson $v_2$ values are compared to the corresponding AMPT model calculations at the same beam energies. Systematic errors on experimental data are shown by the cap symbol.

state of the $s$ and $\bar{s}$ quarks, has a small interaction cross-section with other hadrons, and freezes out early [95, 96]. Due to this small hadronic interaction cross-section of the ϕ meson, its $v_2$ is almost unaffected by later-stage hadronic interactions, and will have a negligibly small value if ϕ mesons are not produced via $s$ and $\bar{s}$ quark coalescence in the partonic phase [97]. Figure 11 shows the $p_T$-integrated ϕ meson $v_2$ for Au+Au collisions as a function of $\sqrt{s_{NN}}$. The $v_2$ values increase with $\sqrt{s_{NN}}$. A comparison with the corresponding $v_2$ values for protons shows that the $v_2$ of ϕ mesons is consistent with that of the protons for $\sqrt{s_{NN}} > 19.6$ GeV. At center-of-mass energies below 19.6 GeV, the average $v_2$ of ϕ mesons seems to deviate from that of protons, as seen in Fig. 11.

The $v_2$ of ϕ mesons is compared to corresponding AMPT model calculations [98, 99] in Fig. 11. The $\langle v_2 \rangle$ values from the model remain constant for all the studied energies for a given parton-parton interaction cross-section, because it arises from the interactions between minijet partons. The $\langle v_2 \rangle$ of ϕ mesons for $\sqrt{s_{NN}} > 19.6$ GeV is consistent with the AMPT model with string melting enabled (AMPT-SM). The AMPT-SM model with a 10 mb parton-parton cross-section fits the data at $\sqrt{s_{NN}} = 62.4$ and 200 GeV, whereas a reduced value of the parton-parton cross-section of 3 mb is needed to describe the data at $\sqrt{s_{NN}} = 27$ and 39 GeV. The ϕ $\langle v_2 \rangle$ data at $\sqrt{s_{NN}} = 11.5$ GeV are consistent with the default framework of the AMPT model without needing partonic interactions.

The comparison with the AMPT model sheds some light on the collision dynamics. It suggests that below $\sqrt{s_{NN}} = 11.5$ GeV, the hadronic interactions may play a significant role, whereas above 19.6 GeV, there may be an increase in the contribution from partonic

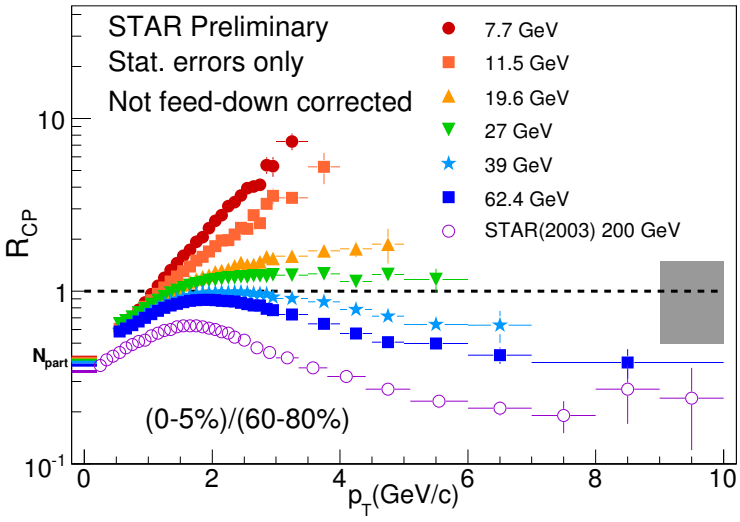


**Figure 12.** Nuclear modification factor versus transverse momentum for inclusive charged hadrons from Au+Au collisions at various $\sqrt{s_{NN}}$ at RHIC. The yield ratios for charged hadrons are taken for 0-5% to 60-80% collision centrality.

interactions.

*2.4.2. Nuclear Modification Factor* One of the most exciting results at RHIC was the discovery of suppression in the production of high transverse momentum ($p_T$) mesons in nucleus-nucleus collisions compared to appropriately scaled $p$+$p$ collisions [74, 72, 100, 101]. This has been interpreted in terms of energy loss of partons in the QGP. This phenomenon is called jet quenching in dense partonic matter [102]. The energy loss by energetic partons in the dense medium formed in high-energy heavy-ion collisions is predicted to be proportional to both the initial gluon density [103, 104] and the lifetime of the dense matter [105]. High-$p_T$ suppression results are usually presented in terms of a nuclear modification factor ($R_{CP}$), defined as

$$R_{CP} = \frac{\langle N_{\rm bin}^{\rm peri}\rangle\, d^3N_{AA}^{\rm cen}/d\eta\, d^2p_T}{\langle N_{\rm bin}^{\rm cen}\rangle\, d^3N_{AA}^{\rm peri}/d\eta\, d^2p_T}, \tag{2}$$

where the $N^{\rm cen}$ and $N^{\rm peri}$ correspond to particle yields in central and peripheral collisions, respectively. The $N_{\rm bin}^{\rm cen}$ and $N_{\rm bin}^{\rm peri}$ are the number of binary collisions for central and peripheral collisions, respectively, commonly estimated from a Glauber model [106].

Figure 12 shows the nuclear modification factor for inclusive charged hadrons from Au+Au collisions at each BES-I energy. The results at high $p_T$ ($> 2$ GeV/$c$) show a smooth transition from strong enhancement at low beam energies to strong suppression at high beam energies. While it is clearly established that the suppression is related to the opacity of a deconfined medium of quarks and gluons, the source of enhancement could have multiple physics interpretations mostly related to dominance of hadronic interactions, like the Cronin

effect, cold matter effects, or strong radial flow. Lack of baseline measurements from $p$+$p$ and $p$+A collisions makes the quantitative interpretation of the measurements at lower beam energies difficult. Hence we need to resort to comparisons with various model-based calculations. On the other hand, it should be noted that PHENIX used $p$+$p$ data sets at 39 and 62.4 GeV to create $R_{AA}$ measurements. These agree qualitatively with the STAR results shown in Fig. 12 [107].

Attempts to compare data to AMPT [98, 99] and HIJING [108] were made and both models failed to reproduce the experimental results. Calculations within the framework of perturbative QCD (pQCD) which focused predominantly, with varying degrees of sophistication, on the implementations of the energy loss of the leading parton or particle in the medium via radiative and collisional processes [109, 110] have explained the high-energy RHIC data to a large extent.

Studying the $R_{CP}$ of identified particles may allow one to separate different effects, although this does limit the $p_T$ reach as seen in Fig. 13. Advanced pQCD calculations [111], which include cold nuclear matter effects, for $R_{CP}$ of identified hadrons [112, 113] in Au+Au collisions for $\sqrt{s_{NN}}$ = 10, 20 and 40 GeV are shown in the upper row of panels of the figure. The model calculations are compared to the corresponding STAR measurements at $\sqrt{s_{NN}}$ = 11.5, 19.6, and 39 GeV. The trend observed in the data is predicted correctly by the model, while the locations where the model predictions cross unity occur at $p_T$ values that are about 1 GeV/$c$ higher than experimentally observed.

The model formalism is based on the QCD factorization approach, augmented by cold nuclear matter and QGP effects. It incorporates the Cronin effect through the multiple elastic scattering of partons in large nuclei, dynamical shadowing through coherent power corrections, and cold nuclear matter energy loss [112, 113]. For the kinematics at hand, the Cronin effect is the most important, and its competition with the QGP energy loss determines the predicted transition from enhancement to suppression for different $\sqrt{s_{NN}}$. The magnitude of nuclear effects is also determined by the steepness of the partonic spectra. Final state energy loss in the QGP is evaluated taking the soft gluon emission limit of full medium-induced splitting kernels [114, 115].

Even though the predictions at all center of mass energies include both the Cronin effect and the energy loss, the net result is an enhancement of $R_{CP}$ at the lowest $\sqrt{s_{NN}}$ = 10 GeV and suppression at high $p_T$ at the highest center of mass energy. The data enhancement over the model predictions at $\sqrt{s_{NN}}$ = 10 GeV could be an indication of the expected change in the medium degrees of freedom from gluon dominated at higest RHIC energies (larger energy losses in the medium compared to quarks and anti-quarks) to quark-antiquark dominated at the lower energies of 7.7 and 11.5 GeV. The difference may allow one to estimate the quark-to-gluon ratio at a particular energy. This is also consistent with the picture of hadronic interactions dominating the system formed in heavy-ion collisions at $\sqrt{s_{NN}}$ = 11.5 and 7.7 GeV. From the comparison with pQCD based calculations, it seems that the enhancement in $R_{CP}$ observed is due to cold nuclear matter effects.

We now proceed to compare the data to a hybrid model [52, 116, 117, 118] where dynamics are dominated by bulk physics and not by jets. This hybrid model is based on

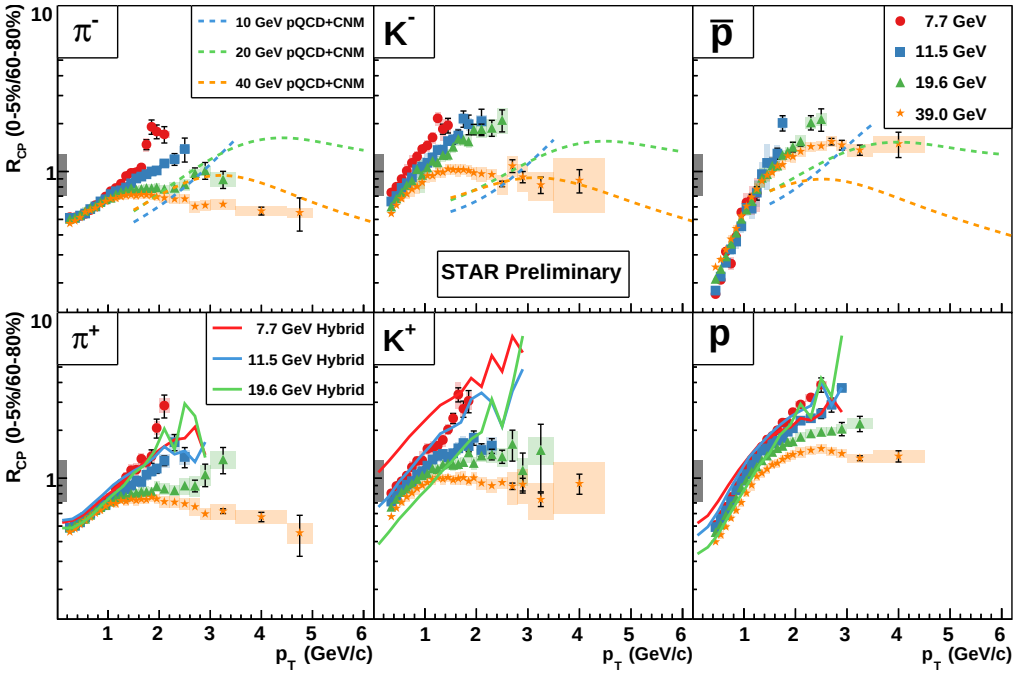


**Figure 13.** STAR data on the nuclear modification factor $R_{CP}$ for π, $K$ and $p$ in Au+Au collisions. The central bin is 0-5% and the peripheral bin is 60-70%. In the upper three panels, pQCD calculations with next-to-leading order accuracy for 10, 20, and 40 GeV are compared to the BES-I data for negatively charged particles. In the lower three panels, Hybrid UrQMD+hydrodynamics calculations [52, 116, 117, 118] for 7.7, 11.5, and 19.6 GeV are compared to the BES-I data for positively charged particles.

the UrQMD transport approach with an intermediate hydrodynamical evolution for the hot and dense stage of the collision. The EOS used in the hydrodynamic part has a crossover for all $\mu_B$ [119]. Event-by-event fluctuations are directly taken into account via the non-equilibrium initial conditions generated by the initial collisions and string fragmentations in the microscopic UrQMD model. After a (3+1)-dimensional ideal hydrodynamic evolution, the hydrodynamical fields are mapped to hadrons via the Cooper-Frye equation and the subsequent hadronic cascade calculations proceed within the UrQMD framework; this incorporates the important final-state effects for a realistic freeze-out.

The lower panels of Fig. 13 compare $R_{CP}$ for charged particles from the Hybrid model with STAR inclusive charged hadrons at $\sqrt{s_{NN}}$ = 7.7, 11.5 and 19.6 GeV. The $p_T$ dependence of $R_{CP}$ at small $p_T$ at these lower beam energies is fairly well captured by the model. The model has stronger radial flow in central collisions compared to peripheral collisions, and this causes the enhancement in $R_{CP}$ for the low energies. This implies that the data at these energies, and in the $p_T$ range reached in BES-I, can be explained purely from a bulk physics perspective, and there is no need for invoking jet physics. With increasing beam energy and $p_T$, jets will become more important, and one then observes the jet quenching effect.

The BES Phase-II program at RHIC, with significantly larger statistics, will allow STAR to reach high enough $p_T$ to conclusively study the hard regime even at $\sqrt{s_{NN}}$ = 11.5 GeV. STAR will study the precise shape of $R_{CP}$ and the position of the crossings at the various energies. This will help to constrain calculations and lead to an understanding of the contributions and interplay between various physical processes (including hard and soft) involved in relativistic heavy-ion collisions.

*2.4.3. Dynamical Charge Correlations* In QCD, chiral symmetry breaking and the origin of hadron masses are related to the existence of topologically nontrivial classical gluonic fields, instantons, and sphalerons, which describe the transitions between the vacuum states with different Chern-Simons numbers. Quark interactions with such fields change the quark chirality and are $\mathcal{P}$ and $\mathcal{CP}$ odd. Such a theoretical proposition had never been observed directly in experiments. It was soon realized that an experimental search for local strong parity violation (LPV) is possible in heavy-ion collisions [120, 121]. For such a phenomenon where the massless quarks can change their chirality due to interactions with gluon fields, there could be separation of positive charges from negative charges along the direction of the angular momentum of the collision, as a result of the large magnetic fields ($\sim 10^{15}$ T) produced in non-central collisions. This phenomenon is also called the chiral magnetic effect (CME) [121, 122, 123]. The CME needs the system to be deconfined, as that allows for the possibility of quarks traveling over distances greater than nucleonic scales, and also requires chiral symmetry restoration, since a chiral condensate will tend to erase any asymmetry between the number of right- and left-handed fermions. Observation of CME at top RHIC energy [124, 125] and its absence at lower beam energy would be considered evidence of a turn-off of one of the QGP signatures.

A three-point correlator, $\gamma \equiv \langle \cos(\phi_\alpha + \phi_\beta - 2\Psi_{\rm RP}) \rangle$, sensitive to the CME was proposed in Ref. [126], where $\phi$ is the azimuthal angle, the subscripts $\alpha$ and $\beta$ denote the particle charge (positive or negative), and $\Psi_{\rm RP}$ is the angle of the reaction plane of a given event. The observable $\gamma$ represents the difference between azimuthal correlations projected onto the direction of the angular momentum vector and correlations projected onto the collision event plane. The STAR measurements [75, 76] of this correlator for Au+Au collisions at 200 GeV shown in Fig. 14(b) demonstrate the "right" ordering of the opposite charge ($\gamma_{\rm OS}$) and the same charge ($\gamma_{\rm SS}$) correlations, supporting the picture of the CME. This is consistent with the formation of deconfined and chirally-symmetric restored matter in high energy heavy-ion collisions. The signal is robust to various ways of determination of the reaction plane [124], and persists when the collision system changes to Cu+Cu [75, 76] or Pb+Pb [125].

An ambiguity in the interpretation of experimental results comes from possible background correlations not related to CME [76]. The background sources, if coupled with collective flow, will also contribute to $\gamma$. Ref. [127] suggests that $(\gamma_{\rm OS} - \gamma_{\rm SS})$ measured by STAR can be explained within a blast wave model that includes charge conservation, with radial and elliptic flow.

Figure 14 presents $\gamma_{\rm OS}$ and $\gamma_{\rm SS}$ correlators for Au+Au collisions at $\sqrt{s_{NN}} = 7.7 - 200$ GeV as a function of centrality. In addition, the ALICE measurements [125] for 2.76 TeV

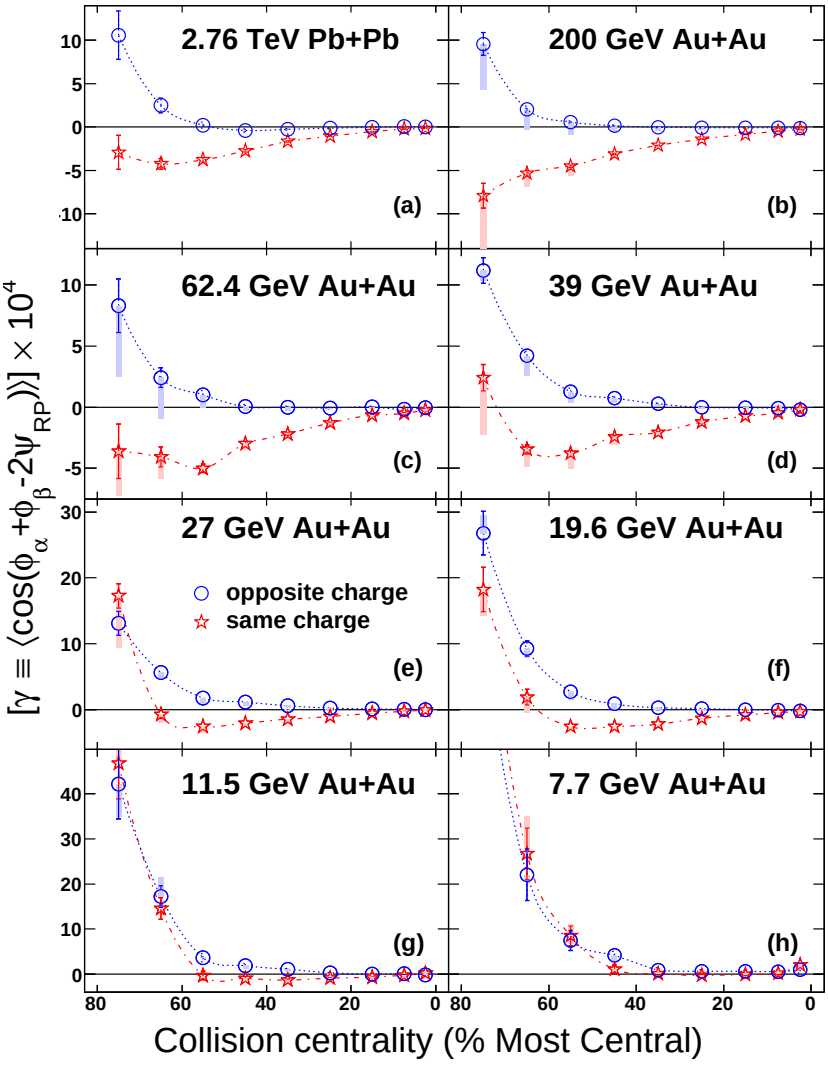


**Figure 14.** The three-point correlator ($\gamma$) as a function of centrality for Au+Au collisions at $\sqrt{s_{NN}}$ = 7.7-200 GeV. Also shown are the corresponding results for Pb+Pb collisions at $\sqrt{s_{NN}}$ = 2.76 TeV from ALICE at the LHC [125]. Note that the vertical scales are different for the different rows. The plotted systematic errors (shaded rectangles) reflect the extra conditions of $\Delta p_T > 0.15$ GeV/$c$ and $\Delta\eta > 0.15$ to suppress HBT + Coulomb effects.

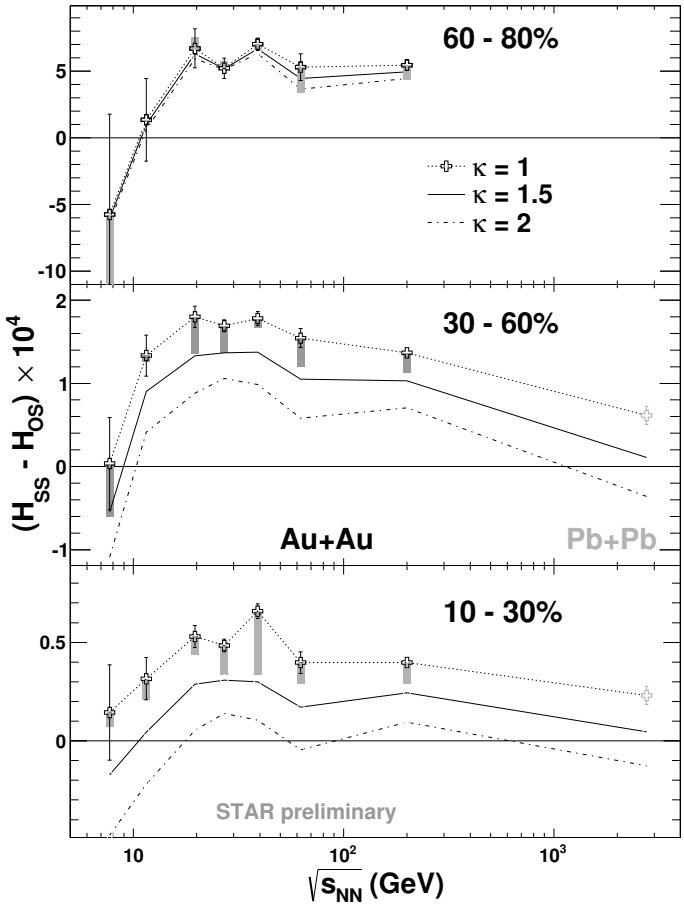


**Figure 15.** $(H_{\rm SS} - H_{\rm OS})$ is shown as a function of beam energy for three centrality bins. The default values (dotted curves) are from $H^{\kappa=1}$, and the solid (dash-dot) curves are obtained with $\kappa = 1.5$ ($\kappa = 2$). For comparison, the results for Pb+Pb collisions at 2.76 TeV are also shown [125]. The plotted systematic errors have the same meaning as in Fig. 14.

Pb+Pb collisions are shown. The ordering of $\gamma_{\rm OS}$ and $\gamma_{\rm SS}$ is present in collisions at the higher energies [75, 76, 125]. This is consistent with extra charge-separation fluctuations perpendicular to the reaction plane due to the CME. At lower beam energies, both $\gamma_{\rm OS}$ and $\gamma_{\rm SS}$ tend to rise for peripheral collisions. This feature seems to be charge independent, and is explained by momentum conservation and elliptic flow [124]. For peripheral collisions, the multiplicity ($N$) is small, and momentum conservation dominates. For more central collisions, where the multiplicity is large enough, this type of $\mathcal{P}$-even background can be estimated by $-v_2/N$ [124, 128].

In order to separate the signal associated with the CME from that due to the background contributions, we can express the experimental observables in the following forms, where the unknown parameter $\kappa$, as argued in Ref. [129], is of the order of unity.

$$\gamma \equiv \langle \cos(\phi_1 + \phi_2 - 2\Psi_{\rm RP}) \rangle = \kappa v_2 F - H \tag{3}$$

$$\delta \equiv \langle \cos(\phi_1 - \phi_2) \rangle = F + H\,, \tag{4}$$

where $H$ and $F$ are the CME and background contributions, respectively. Figure 15 shows $H_{SS} - H_{OS}$ as a function of beam energy for three centrality bins in Au+Au collisions. The default values (dotted curves) are from $H^{\kappa=1}$, and the solid (dash-dot) curves are obtained with $\kappa = 1.5$ ($\kappa = 2$), where $\kappa$ is a parameter that could account for finite detector acceptance and for theoretical uncertainties. For comparison, results for $10-60\%$ Pb+Pb collisions at 2.76 TeV are also shown [125]. In the case of $\kappa = 1$, $(H_{SS} - H_{OS})$ demonstrates a weak energy dependence above 19.6 GeV, and trends toward zero at the lowest beam energy, although the statistical errors are large for 7.7 GeV. This may be explained by the probable dominance of hadronic interactions over partonic ones at the lowest energies. With increased $\kappa$, $(H_{SS} - H_{OS})$ decreases for all beam energies and may even totally disappear in some cases (e.g. with $\kappa \sim 2$ in $10-30\%$ collisions). If better theoretical estimates of $\kappa$ are available in the future, a more conclusive result could be extracted from Fig. 15 with interpolation or extrapolation of the data. The energy for which $(H_{SS} - H_{OS})$ = 0 will be determined quantitatively with higher statistics in BES Phase-II.

*2.4.4. Chiral Transition and Dileptons* Electromagnetic observables, such as photons and dileptons, are ideal probes that are emitted throughout the evolution of a heavy-ion collision, thus carrying information about all the stages of the reaction [130, 131]. As leptons are inert to the strong force, there will be negligible interactions in the medium, hence they are considered to be ideal penetrating probes. Apart from Dalitz decays, prominent sources of dileptons in the low invariant-mass range (LMR: $M_{ee} < 1.1$ GeV/$c^2$) are direct leptonic decays of the $\rho(770)$, $\omega(782)$, and $\phi(1020)$ vector mesons. The $\rho$ meson is of special interest given that in thermal equilibrium, its contribution to the low mass range is expected to dominate through its strong coupling to the $\pi\pi$ channel. Moreover, its short lifetime $\tau = 1.3$ fm/$c$ makes its spectral shape especially sensitive to in-medium modifications, a proposed signature of chiral symmetry restoration [132].

At SPS energies, the apparent low-mass dilepton enhancement observed in both the CERES dielectron [133] and NA60 dimuon data [134] can be explained in terms of in-medium modifications of the spectral shape of the $\rho$ meson. The dimuon measurements by NA60 are found to favor significant broadening of the $\rho$ meson line shape over a mass-dropping scenario [135, 136, 137, 138]. At top RHIC energies ($\sqrt{s_{NN}}$ = 200 GeV), both the PHENIX [139] and STAR [140] collaborations have observed a significant enhancement in the low-mass dielectron measurements. Models that have been able to describe the measurements at SPS energies can describe the enhancements seen at RHIC, with the exception of results from PHENIX for the most central collisions.

Dilepton measurements in the intermediate invariant mass range (IMR), typically defined to be between the masses of the $\phi$ and J/$\psi$ mesons, are sensitive to thermal radiation from the QGP [4]. However, contributions from semi-leptonic decays of open heavy-flavor hadrons are significant for the higher RHIC beam energies. In the BES-I program, such direct measurements could not be performed. With STAR's recently improved muon detection capabilities, however, direct measurements of $e$-$\mu$ correlations should in the future help establish the open heavy-flavor contributions.

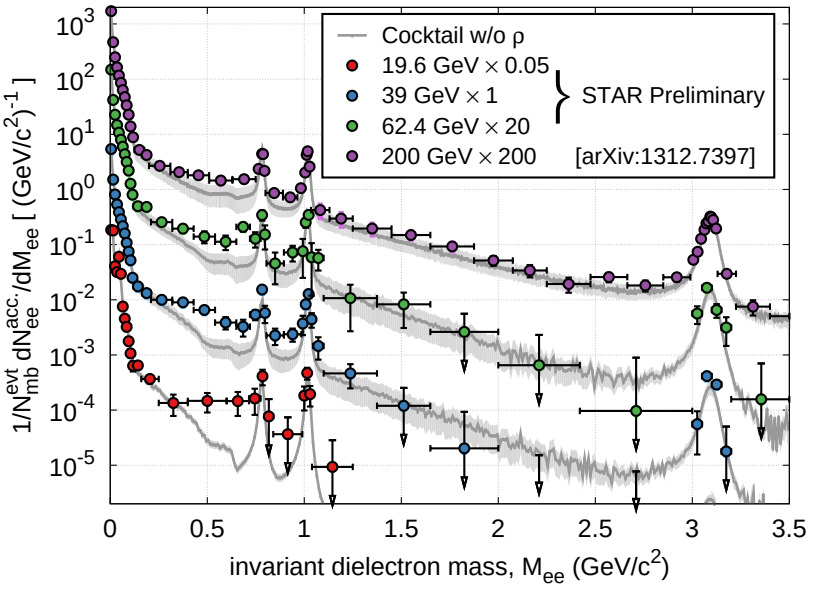


**Figure 16.** Background-subtracted dielectron invariant-mass distributions from Au+Au collisions at $\sqrt{s_{NN}}$ = 19.6, 39, 62.4, and 200 GeV. The (colored) dotted lines show the hadron cocktails (excluding contributions from ρ mesons). The (color) shaded areas indicate systematic uncertainties.

The BES-I program has put STAR in a unique position to systematically measure dielectron spectra in the low and intermediate mass ranges from SPS center-of-mass energies to the top RHIC energies, $\sqrt{s_{NN}} = 200$ GeV. Figure 16 shows the dielectron invariant mass distributions extending out to the J/ψ mass for minimum-bias (0 - 80%) Au+Au collisions at beam energies from $\sqrt{s_{NN}}$ =19.6 up to 200 GeV. Dielectron measurements are statistically challenging due to very low signal-to-background ratios. Compared to a total minimum-bias sample of about 770M events at $\sqrt{s_{NN}} = 200$ GeV (Fig. 16 only involves 260M events) BES-I only reached 36M, 130M, and 67M events, for $\sqrt{s_{NN}}$ =19.6, 39, and 62.4 GeV, respectively (see Table 1). Consequently, in the intermediate mass range, the statistical uncertainty for the lower beam energies is very large, and complicates a meaningful interpretation of the results.

In Fig. 17, the efficiency-corrected invariant mass spectra are shown for minimum-bias Au+Au collisions at $\sqrt{s_{NN}}$ = 19.6, 39, 62.4, and 200 GeV. The hadron cocktail simulations include contributions from Dalitz decays and dielectron decays of the ω and ϕ vector mesons. Contributions from ρ mesons have been excluded from the cocktail, but are explicitly included in the model calculations in [141]. It has been noted that while the free emission rates of dileptons in the QGP and hadron gas phase are very different, the in-medium rates in both phases approach each other when extrapolated into the expected phase transition region [142]. It was also noted in Ref. [143] that the degeneracy of the top-down extrapolated pQCD and the bottom-up hadronic many-body calculations indirectly implies chiral symmetry restoration, since in pQCD, the vector and axial vector components are degenerate. When compared with the experimental results, the model calculations provide a robust description from top RHIC

energies down to SPS energies. Furthermore, this observation agrees with the expectation that medium effects are driven by the strong coupling to baryons, and thus to the total baryon density, since the ρ mesons interact symmetrically with baryons and antibaryons [144].

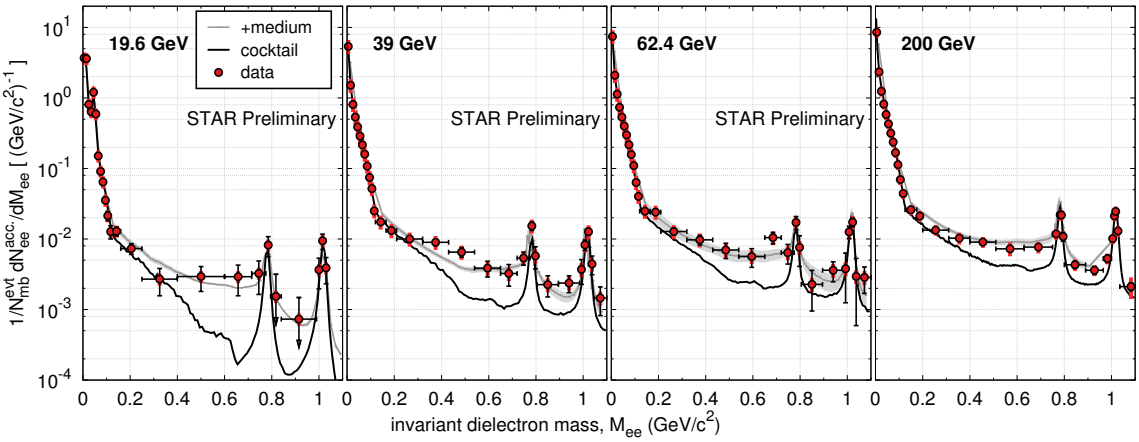


**Figure 17.** BES-I dielectron invariant mass distributions in the low invariant-mass range from Au+Au collisions at $\sqrt{s_{NN}} = 19.6$, 39, 62.4, and 200 GeV. The 39 and 62 GeV measured spectra have both been scaled to the cocktail $\pi^0$ yields. The black curves depict the hadronic cocktail and include all known hadronic sources with the exception of the ρ meson. The grey curves depict model calculations [141] which include contributions from both the hadron gas and QGP phases.

At SPS beam energies, with substantial nuclear stopping, most baryons are participating nucleons. At RHIC top energies, on the other hand, the net-baryon density largely vanishes, while a significant baryon-antibaryon production is expected to compensate the total baryon density. The total baryon density at freeze-out as a function of $\sqrt{s_{NN}}$, as shown in Fig. 18, does not change significantly with center-of-mass energies above 20 GeV. Accordingly, models that show good agreement at SPS and top RHIC energies should be able to describe the low-mass enhancement throughout the BES-I energy range.

STAR's systematic LMR dielectron measurements during BES-I allowed models to tie recent results at top RHIC energies to (top) SPS energies. The preliminary results illustrate how the measured excess develops as a function of the beam energy while the total baryon density remains approximately similar as can be seen in Fig. 18 [**?**]. Taking the measurements to beam energies below 19.6 GeV would provide further opportunity to compare to SPS measurements [133] at 40 *A* GeV fixed-target energies.

While the LMR measurements provide a way to study the chiral symmetry restoration, the duality of the dilepton rates around $T_c$ will make it difficult to separate the relative contributions from the QGP or hadron gas phases. Instead, with its blue-shift-free invariant mass slope, the IMR is sensitive to changes of $T_c$. Using the relation between the real photon and virtual photon production, measured via the associated dielectric production, one can study the properties of the QGP. In addition, for $p_T > 6$ GeV/$c$, one can also study the photon production in the primordial phase of the collision. The limited statistics collected during BES-I was too small for meaningful measurements in the intermediate mass range.

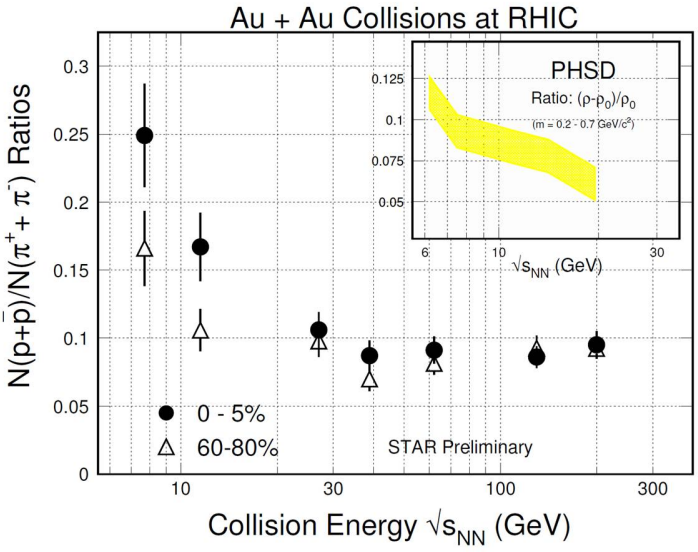


**Figure 18.** STAR measurements of $(p+\bar{p})/(\pi^+ + \pi^-)$ in Au+Au collisions as a function of the center-of-mass energy $\sqrt{s_{NN}}$ are shown for the 0-5% (circles) and 60-80% (triangles) centralities. The shaded area in the in-set indicates PHSD model predictions for the in-medium ρ yield as determined in the invariant dielectron mass range of 0.2 to 0.7 GeV/$c^2$ in minimum-bias Au+Au collisions [146].

One of the most important objectives of the beam energy scan is the search for the critical point. A system close to the critical point will see an increase in its correlation lengths, and hence relaxation rates will exhibit critical slowing down. Because total dilepton yields are sensitive to the duration of emission, an *anomalous* increase in the lifetime of the fireball would be detectable through an increase in the dilepton yields [147]. It should be noted that in some models, the critical slowing down is completely governed by soft hydro modes and this complicates the relationship between the lifetime of the system and the dilepton yields. With an accuracy of $\pm 1$ fm/$c$, NA60's lifetime measurements [148] at $\sqrt{s_{NN}} = 17.3$ GeV did not provide any evidence of such anomalous increases in a notably smaller system of In+In collisions. However, in model calculations, most EM radiation occurs around $T_c$, thus making the dilepton channel sensitive for lifetime changes that occur around this region. Consequently, a change in lifetime of 25% could result in a yield increase up to 40%.

### *2.5. Summary of BES-I*

The BES-I program at STAR had the following goals: (a) to carry out a search for threshold energies for the signatures of QGP already established at $\sqrt{s_{NN}} = 200$ GeV, corroborating the discovery of QGP; (b) to search for signatures of a first-order phase transition; and (c) to search for a critical point at high $\mu_B$. Towards achieving these goals, Au+Au data were collected by STAR in 2010 and 2011 at 6 energies ($\sqrt{s_{NN}}$ = 7.7, 11.5, 19.6, 27, 39, and 62.4 GeV). Data at the final BES-I energy, 14.5 GeV, were collected in February and March of 2014.

Analysis of the yields of several hadron species ($\pi^{\pm}$, $K^{\pm}$, $K^0_S$, $p$, $\overline{p}$, $\phi$, $\Lambda$, $\overline{\Lambda}$, $\Xi$, $\overline{\Xi}$, $\Omega$,

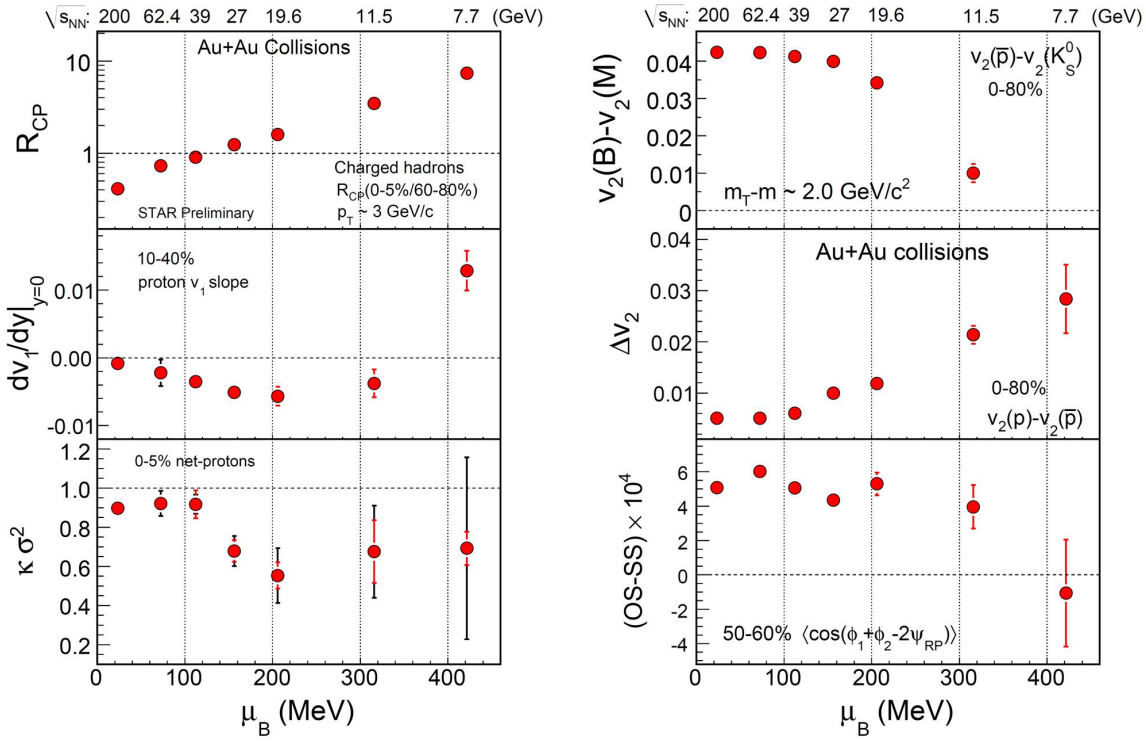


**Figure 19.** A summary of selected results from Au+Au collisions in the BES-I program at RHIC as a function of baryon chemical potential. The left panel shows midrapidity results for the nuclear modification factor for $p_T \sim 3$ GeV/$c$ for charged hadrons, the slope of directed flow of protons for 10-40% centrality, and $\kappa\sigma^2$ for net-protons for 0-5% centrality. The right panel shows results for the difference in baryon and meson $v_2$ at $m_T - m = 2$ GeV/$c^2$ for minimum-bias collisions, the difference between $v_2$ of protons and antiprotons for minimum-bias collisions, and the difference between opposite-sign and same-sign charge correlations with respect to the reaction plane for 50-60% centrality. Note that the connection to $\mu_B$ is not exact, as the $\mu_B$ assignment at a given collision energy is dependent on the centrality, and the various analyses have different centrality selections.

and $\overline{\Omega}$) suggest that the RHIC BES-I program covered a $\mu_B$ range from 20 MeV to about 420 MeV in the QCD phase diagram. Lattice-based QCD calculations indicate that this $\mu_B$ range could capture key phase features like the critical point and the region of the first-order phase transition.

A summary of several interesting observations reported here is presented in Fig. 19. All observables exhibit interesting trends as a function of $\mu_B$ as the beam energy is changed from 7.7 GeV to 200 GeV. The nuclear modification factor ($R_{CP}$) for charged hadrons in 0-5% central Au+Au collisions at $p_T \sim 3$ GeV/$c$ changes from below unity at $\mu_B$ = 20 MeV ($\sqrt{s_{NN}}$ = 200 GeV) to above unity for $\mu_B$ = 155 MeV ($\sqrt{s_{NN}}$ = 27 GeV). This suggests a reduction in the partonic energy loss. However, higher $p_T$ must be reached in order to map out the interplay between hard scatterings and the effects of soft physics or cold nuclear matter. The slope of the directed flow of protons ($dv_1/dy$) in mid-central collisions (10-40%

centrality) near midrapidity shows a clear non-monotonic variation with respect to $\mu_B$ ($\sqrt{s_{NN}}$). The minimum value of $dv_1/dy$ lies above $\mu_B$ = 205 MeV (below $\sqrt{s_{NN}}$ = 19.6 GeV). This observable, which is driven by the pressure gradients developed in the system, is sensitive to possible first-order phase transition effects, but BES-I statistics are insufficient to map-out the apparent strong centrality dependence of the phenomenon. The $\kappa\sigma^2$ of the net-proton number distribution shows an interesting variation with $\mu_B$ ($\sqrt{s_{NN}}$). Current statistics are insufficient to clarify whether the trend follows a non-monotonic variation, with a minimum between $\mu_B$ = 155 to 315 MeV ($\sqrt{s_{NN}}$ = 27 to 11.5 GeV) as observed for the proton $dv_1/dy$, or a monotonic variation with $\mu_B$ ($\sqrt{s_{NN}}$). The right panel of Fig. 19 shows that the difference in the $v_2$ of baryons and mesons in minimum-bias Au+Au collisions at $m_T$ - $m \sim 2$ GeV/$c^2$ decreases with increasing $\mu_B$ (decrease in $\sqrt{s_{NN}}$). This difference starts to decrease after $\mu_B$ = 155 MeV ($\sqrt{s_{NN}}$ = 27 GeV). The existence of a difference between the $v_2$ of baryons and mesons at intermediate $p_T$ is the key to the experimental observation of NCQ scaling and the observation of partonic collectivity at top RHIC energy. The most telling particle for this analysis is the $\phi$, which is a meson with the mass of a baryon. The statistical error on the BES-I $\phi$ $v_2$ data preclude quantitative conclusions. It is also observed that the difference in $v_2$ between baryons and antibaryons (shown for protons and antiprotons in minimum-bias Au+Au collisions at midrapidity in Fig. 19) starts to increases with $\mu_B$ (decreases with $\sqrt{s_{NN}}$). Comparison to model calculations suggests that these observations are consistent with the finding that hadronic interactions dominate at lower beam energies. Finally, the difference in the observed signal of dynamical charge correlations between same-sign and opposite-sign charges for 50-60% central Au+Au collisions at midrapidity as a function of $\mu_B$ ($\sqrt{s_{NN}}$) is shown. One of the possible explanations for this difference at top RHIC energy is the Chiral Magnetic Effect. This would imply the formation of a deconfined state of quarks and gluons with chiral symmetry restored. The observed trend towards a vanishing of this difference then could indicate the absence of such a deconfined state in the systems at lower beam energies. Although there is a trend towards a vanishing difference, it is really only the 7.7 GeV data point which shows no difference. However, the statistical error bars make it difficult to draw strong conclusions, and it is not possible to quantitatively estimate the beam energy at which the onset of deconfinement is achieved.

The dilepton invariant-mass spectrum has promise for revealing the nature of hadronic structure in the vacuum, and insights into chiral symmetry restoration with increasing temperature and/or total baryon density. The dielectron measurements from BES-I only provide enough statistics for studies in the higher energy range $\sqrt{s_{NN}} \geq 20$ GeV. Model calculations are consistent with results from heavy-ion collisions at SPS and at various RHIC energies. These calculations indicate that the observed excess yields in the low mass range could be attributed to $\rho$-meson broadening, driven by the total baryon density in the medium, while the thermal radiation from the partonic phase dominates the intermediate mass range. The programs at RHIC at 200 GeV and at the LHC will untangle thermal radiation and open heavy-flavor contributions in the intermediate-mass range. At lower energies, corresponding to higher baryon densities, the intriguing puzzle concerning the source of the excess yields in the low mass range remains to be addressed.

## 3. Proposal for BES Phase-II

### *3.1. Physics Objectives and Specific Observables*

The BES-I scientific program has localized the most interesting regions and has identified the observables which are likely to be the most discriminating for understanding the QCD phase structure. However, several of the key measurements were found to require higher statistics in order to provide a quantitative physics conclusion. Therefore, we propose to run a second phase of the beam energy scan (BES Phase-II) which is driven by the precision requirements of this suite of physics observables. The bullets below provide an overview of the observables key to achieving the goals of the BES Phase-II program. Following those bullets are subsections detailing the requirements and expected resolution that will be reached for each key observable.

- **Onset of QGP:** Measurements to be carried out include: the nuclear modification factor as a function of $p_T$ for produced hadrons, azimuthal anisotropy measurements as a function of $p_T$ for the identified hadrons with particular emphasis on the $\phi$ meson and the multi-strange hyperons, and the centrality dependence of charged particle correlations with respect to the reaction plane. Our current measurements show interesting trends in these measurements as a function of center-of-mass energies, and they point towards a possible turn-off of the signals of QGP below 19.6 GeV.
  The nuclear modification factor at high $p_T$ having a value below unity is regarded as a signature of formation of hot and dense matter of quarks and gluons. Current measurements below 27 GeV do not have sufficient event statistics to extend in $p_T$ to 5 GeV/$c$, thereby preventing a quantitative conclusion on the turn-off of this signal of QGP. In the azimuthal anisotropy measurements, the $v_2$ of $\phi$ mesons plays a crucial role. Since generation of a large $v_2$ of $\phi$ mesons requires partonic interactions prior to the formation of $\phi$, an absence or a low value of $v_2$ of $\phi$ mesons compared to other hadrons could indicate that the system created in heavy-ion collisions does not undergo the quark-hadron phase transition. Current measurements of $v_2$ of $\phi$ mesons versus $p_T$ at 11.5 and 7.7 GeV provides such an indication, but with large statistical errors on the data points. A high statistics measurement of $v_2$ of $\phi$ mesons versus $p_T$ is crucial in order to find out if a turn-off of partonic collectivity occurs below 19.6 GeV. The centrality dependence of a finite difference in charge correlations with respect to the reaction plane for same- and opposite-charge pairs is considered a signature of the Chiral Magnetic Effect. Within large statistical uncertainties, this difference is consistent with zero in BES-I measurements at 7.7 GeV. Since one of the prerequisites of this phenomenon is the formation of a partonic phase, a statistically significant null result at lower beam energies will be an observation of turn-off of QGP. With the higher event statistics of the BES Phase-II program further effects of the chiral magnetic wave, such as the chiral separation effect [149, 150] and the chiral vortex effect [151] can also be studied.
- **First-order phase transition:** The relevant measurements include the slope of rapidity dependence of directed flow for protons and net-protons, and tilt angle of the source

as measured through azimuthally sensitive femtoscopy. A minimum in $dv_1/dy$ versus center of mass energy has been argued to indicate the softest point in the EOS of the system formed in heavy-ion collisions. A statistically significant measurement has been obtained in BES-I, but the location of the minimum energy point has not been fixed precisely. Current measurements suggest that it lies somewhere between the energy values of 19.6 and 11.5 GeV, corresponding to a $\mu_B$ difference of more than 100 MeV. Furthermore, differential measurements of this observable, like as a function of collision centrality at different beam energies and for different baryon and meson species, would provide additional data to refine this signature of a first-order phase transition. These additional measurements require increased statistics compared to BES-I. The tilt of the emission source is also proposed to have sensitivity to the softest point in the EOS. This observable is a new measurement unique to BES Phase-II. A measurement of this observable was not possible with the BES-I data to the high statistics demands of the azimuthally sensitive femtoscopy analysis which is necessary to infer coordinate space anisotropies.

- **Critical Point:** A non-monotonic variation of the product of high moments for net-protons, specifically the $\kappa\sigma^2$ with beam energy has been considered in the literature as a signal for a CP. The current measurements indicate that the trend of net-$p$ $\kappa\sigma^2$ is flat from 200-39 GeV. Starting at 27 GeV, the values of $\kappa\sigma^2$ of net-$p$ show a clear drop. However the statistical errors on the measurements at 11.5 and 7.7 GeV are too large for the purpose of further gauging the energy dependent variations at the lower energies. A high statistics measurement of the possible rise in the $\kappa\sigma^2$ values at energies below 19.6 GeV would open up an exciting opportunity to study the QCD critical point physics at RHIC.
- **Chiral Phase Transition:** High statistics dilepton measurements to date provide the most powerful observable to understand in-medium effects and a possible chiral phase transition. While in the low mass region (around and below the $\rho$ mass) there is the possibility of investigating symmetry restoration, the intermediate mass region allows a possible temperature measurement of the partonic phase. The BES program has clearly demonstrated STARs capability for such measurements for energies as low as 19.6 GeV. The results obtained so far are consistent with formation of a partonic phase, with partial restoration of chiral symmetry, and suggest the importance of baryon-dominated interactions in affecting the $\rho$ meson spectra [152, 153, 154, 155]. BES Phase-II will offer a great new opportunity to make a high-statistics measurement of dileptons at energies below 27 GeV to see the effect of the possible turn-off of QGP and the increased baryonic interactions in the system.

In Table 2 we outline the statistics requires to make a precision measurement of each proposed observable at each proposed energy. In the subsections that follow, we discuss each proposed observable in more detail, we decribe the precision necessary for a conclusive measurement, and we present the projected errors expected after the BES Phase-II program.

**Table 2.** Event statistics (in millions) needed for Beam Energy Scan Phase-II for various observables.

| Collision Energy (GeV) | 7.7 | 9.1 | 11.5 | 14.5 | 19.6 |
|---|---|---|---|---|---|
| $\mu_B$ (MeV) in 0-5% central collisions | 420 | 370 | 315 | 260 | 205 |
| Observables | | | | | |
| $R_{CP}$ up to $p_T$ = 5 GeV/$c$ | – | | 160 | 125 | 92 |
| Elliptic Flow ($\phi$ mesons) | 100 | 150 | 200 | 200 | 400 |
| Chiral Magnetic Effect | 50 | 50 | 50 | 50 | 50 |
| Directed Flow (protons) | 50 | 75 | 100 | 100 | 200 |
| Azimuthal Femtoscopy (protons) | 35 | 40 | 50 | 65 | 80 |
| Net-Proton Kurtosis | 80 | 100 | 120 | 200 | 400 |
| Dileptons | 100 | 160 | 230 | 300 | 400 |
| **Required Number of Events** | **100** | **160** | **230** | **300** | **400** |

*3.1.1. $R_{CP}$ of identified hadrons up to $p_T$ = 5 GeV/c* High-$p_T$ suppression is seen as an indication of the energy loss of leading partons in a colored medium. Therefore, the $R_{AA}$ measurements are one of the clearest signatures for the formation of the quark-gluon plasma. Because there was not a comparable $p+p$ energy scan, the BES analysis has had to resort to $R_{CP}$ measurements as a proxy. Still the study of the shape of $R_{CP}(p_T)$ will allow us to quantitatively address the evolution of the phenomenon of jet-quenching to lower beam energies. A very clear change in behavior as a function of beam energy is seen in these data (see Figs. 12 and 13); at the lowest energies (7.7 and 11.5 GeV) there is no evidence of suppression for the highest $p_T$ values that are reached. However, it should be noted that for these energies the BES-I measurements are only able to reach 3-4 GeV/$c$ for inclusive hadrons and 2-3 GeV/$c$ for identified hadrons. Typically, one considers $p_T$ of 5 GeV/$c$ and above to be dominated by partonic behavior. Therefore, although the BES-I $R_{CP}$ results are suggestive of a disappearance of this QGP signature, they are not conclusive. The $p_T$ reach expected in the proposed BES Phase-II measurements will be crucial in drawing definitive conclusions about evidence for the creation of QGP at a given collision energy.

Although the BES-I spectra do not reach high enough $p_T$ to extend into the purely hard-scattering regime, they do allow us to make detailed projections of how many events would be needed to reach a given $p_T$ for a given beam energy. We propose to acquire about 400 tracks in the $p_T$ range of 4-5 GeV/$c$ for the 11.5, 14.5, and 19.6 GeV energies. At the lower energies of 7.7 and 9.1 GeV, there is simply not enough kinematic reach to get out to 4-5 GeV/$c$. These required numbers of events are listed in Table 2

We have used the yields of identified particles measured in BES-I to make projections of the expected errors for the $R_{CP}$ measurements with increased statistics expected to be available in BES Phase-II. For each particle species, energy, and centrality, we have used a exponential extrapolation (note that this is a more conservative estimate than the power law extrapolation) to estimate the expected number of particles to be measured in each $p_T$ bin based on the expected number of events at each energy shown in Table 2. From this expected number of particles per bin, we can estimate the statistical error for the central and peripheral bins and propagate these to estimate the expected error on the $R_{CP}$ measurements. These projected

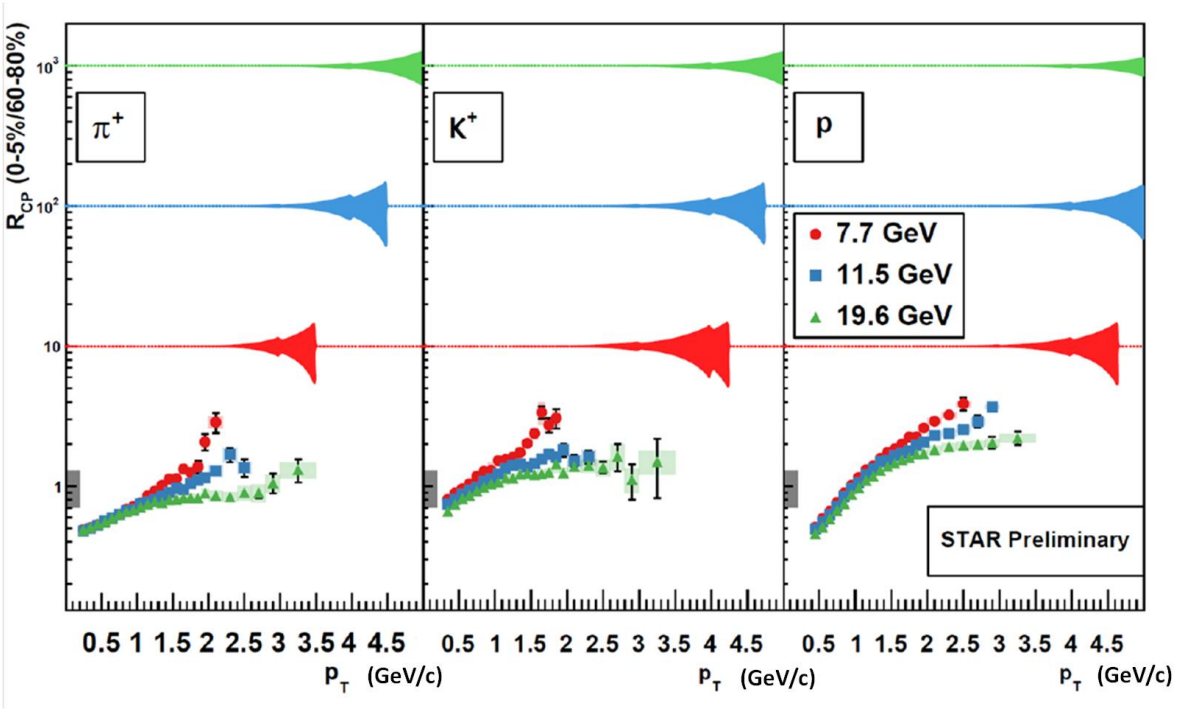


**Figure 20.** The BES-I $R_{CP}$ data are are shown for π, $K$, and $p$ for 7.7, 11.5, and 19.6 GeV. The BES Phase-II projected error bands are for the same energies, 7.7 (red, scaled by 10), 11.5 (blue, scaled by 100), and 19.6 (green, scaled by 1000).

errors are displayed in Fig. 20 as colored bands. For clarity of presentation, the projected error bands are scaled by 10 (for 7.7 GeV), 100 (for 11.5 GeV), and 1000 (for 19.6 GeV). The error bands are truncated when the error reaches 50%; this represents the expected high $p_T$ limit for each measurement. For intermediate energies the expected error bands can be interpolated. It is also of interest to consider the inclusive charged hadron $R_{CP}$ measurement (Fig. 12). We have also projected the expected error in BES Phase-II for this measurement, therefore, we can report the high $p_T$ limits for the inclusive charged hadron $R_{CP}$ are found to be 5.2, 5.7, and 6.5 GeV/c for the 7.7, 11.5, and 19.6 GeV systems, respectively.

*3.1.2. The $v_2$ of ϕ mesons and NCQ scaling for indentified particles* This measurement will allow us to quantitatively address the suspected decrease, followed by an absence, of partonic collectivity below $\sqrt{s_{NN}}$ = 19.6 GeV. High-statistics data with a new event plane detector (as discussed below in section 3.6) are required. It is necessary to make measurements up to $p_T$ = 3 GeV/$c$ with a statistical error of less than 10% on $v_2$. From this resolution requirement we can estimate the statistics necessary (see Table 2) for BES Phase-II to reach transverse momenta beyond 2.5 GeV/c even at the lowest energies. This will allow us to test in NCQ scaling detail for many particle species, including multi-strange particles.

The projection of the statistical errors for the ϕ meson $v_2$ for BES Phase-II are shown by the shaded bands in both plots in Fig. 21. The shapes of the kaon $v_2(p_T)$, dashed line, were

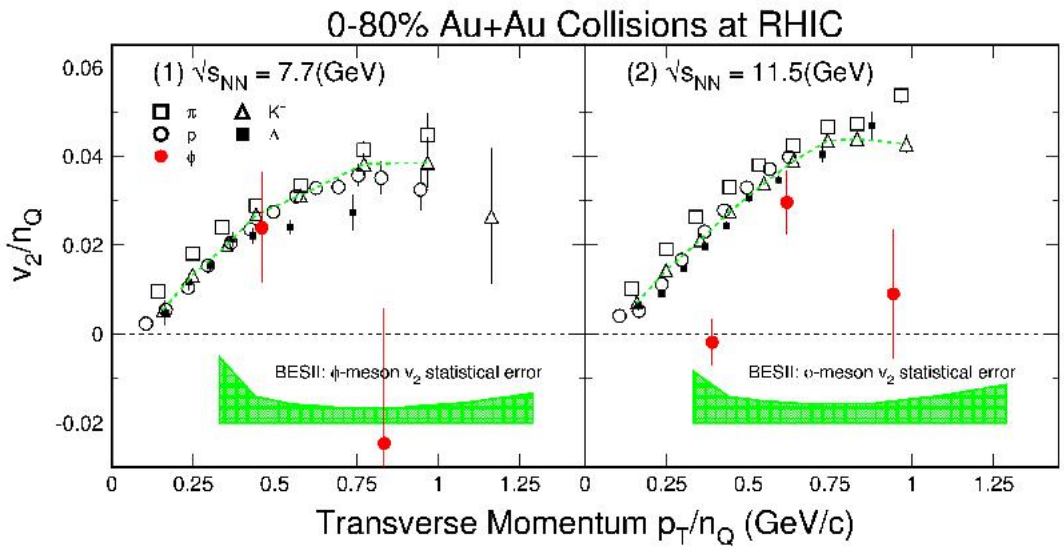


**Figure 21.** Number of constituent quark (NCQ) scaled event anisotropy parameter ($v_2$) for identified hadrons, including the $\phi$-meson (filled circles) from minimum bias (0-80%) Au+Au collisions at 7.7 GeV (left) and 11.5 GeV (right). The projections of the statistical errors for the $\phi$-meson $v_2$, from BES Phase-II are shown by the shaded bands in both plots. The shapes of the kaon $v_2(p_T)$, dashed line, were used in the estimation.

used in the estimation. As shown in Table 2, 100M and 200M useful minimum bias events are requireded from the Au+Au collisions at 7.7 and 11.5 GeV, respectively. The shape of the kaon $v_2$ is assumed for the estimation up to $p_T \approx 3$ GeV/$c$ where the scaling has been observed in high-energy nuclear collisions at the RHIC energies [34] in both plots. These measurements will answer decisively the question how much $\phi$ meson flow there is compared to that of light quark hadrons. Lack of the collectivity of the $\phi$ meson will provide clear evidence of the hadronic interaction dominated medium in the low energy heavy ion collisions. Moreover, with such statistics, information of the event anisotropy parameters for multi-strange hadrons, such as $\Xi$ and $\Omega$, can also be extracted.

*3.1.3. Three-particle correlators related to CME/LPV* These measurements will allow us to corroborate the observation of the turn-off of CME/LPV-like effects at 7.7 GeV. In order to reduce the statistical error on the measured CME signal $H_{SS} - H_{OS}$ by a factor 3 as shown in Fig. 22, we propose to increase the event statistics by factors of ten and four at 7.7 and 11.5 GeV, respectively. This requires $\sim$ 50M events for each beam energy (see Table 2).

Besides the chiral magnetic effect, the chiral separation effect (CSE) has also been proposed. The CSE refers to the separation of chiral charge along the axis of the magnetic field at finite density of vector charge (e.g., electric charge) [149, 150]. In a chirally-symmetric phase, the CME and CSE form a collective excitation, a Chiral Magnetic Wave (CMW), a long-wavelength hydrodynamic mode of chiral charge densities [156, 157]. The CMW is a signature of chiral symmetry restoration in the QGP, and manifests itself in a finite electric

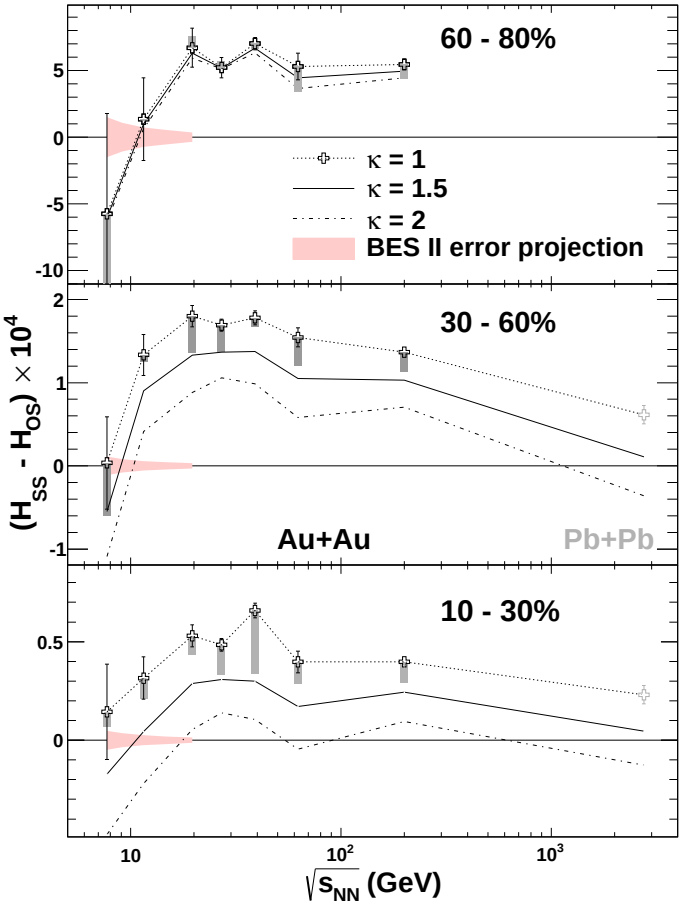


**Figure 22.** The $(H_{SS} - H_{OS})$ difference as a function of beam energy is now shown with error projections for BES Phase-II.

quadrupole moment of the collision system, where the "poles" ("equator") of the produced fireball acquire additional positive (negative) charge. This effect, if it exists, will be reflected in the measurement of charge-dependent elliptic flow. Taking pions as an example, on top of the baseline $v_2^{\rm base}(\pi^{\pm})$, the CMW will lead to [156]

$$v_2(\pi^{\pm}) = v_2^{\rm base}(\pi^{\pm}) \mp (\frac{q_e}{\bar{\rho}_e})A_{\rm ch}, \tag{5}$$

where $q_e$, $\bar{\rho}_e$ and $A_{\rm ch} = (N_+ - N_-)/(N_+ + N_-)$ are the quadrupole moment, the net charge density, and the charge asymmetry of the collision event, respectively. The baseline $v_2$ may be different for $\pi^+$ and $\pi^-$ because of several other physics mechanisms [158, 159], so it is less ambiguous to study the CMW via the $A_{\rm ch}$ dependence of pion $v_2$.

Taking 30-40% central 200 GeV Au+Au for example, the pion $v_2$ was shown as a function of $A_{\rm ch}$ in the left panel of Fig. 1 in Ref. [160]. The $\pi^-$ $v_2$ increases with $A_{\rm ch}$ while the

$\pi^+$ $v_2$ decreases with a similar magnitude of slope. The $v_2$ difference between $\pi^-$ and $\pi^+$ was fitted with a straight line in the right panel of the referenced figure. The slope parameter $r$, or presumably $2q_e/\bar{\rho}_e$ from Eq. 5, is positive and qualitatively consistent with the expectation of the CMW picture. We retrieved the slope parameter $r$ for all centrality bins, as shown in Fig. 2 in Ref. [160]. The slopes are consistent with zero for the most central and most peripheral collisions, and are positive and reach a maximum in mid-central/mid-peripheral collisions. For Au+Au collisions at 200 GeV, the slopes extracted from UrQMD [161] events are consistent with zero for the 10-70% centrality range, where the signal from the real data is prominent. On the other hand, simplified CMW calculations [162] demonstrate a similar centrality dependence of the slope parameter.

The STAR preliminary results show a similar trend and magnitude of the slopes for Au+Au collisions from 200 GeV to 19.6 GeV, where the statistical errors become large enough to prevent a firm conclusion. With the proposed numbers of events for the BES Phase-II, we will be able to reduce the statistical errors, and further search for the CMW at lower energies. The possible disappearance of the CMW at lower energies would signify chiral symmetry breaking.

In addition to the chiral magnetic effect, a chiral vortical effect (CVE) has also been predicted [151]: the fluid vorticity $\vec{\omega}$, combined with a baryon chemical potential $\mu_B$, creates an effective magnetic field $\mu_B\vec{\omega}$. Vorticity in heavy-ion collisions is a natural consequence of angular momentum conservation. There will be a baryon number separation due to the CVE in analogy with the electric charge separation due to the CME. Indeed, recent STAR preliminary results for $\Lambda-$proton correlations [163] show the separation between opposite- and same-baryon number correlators ($\gamma$) in Au+Au collisions at 200 GeV. The statistics requested for BES Phase-II will enable such an analysis at lower energies, where the relative importance of baryon number separation increases with decreased beam energy of collisions where $\mu_B$ is larger.

*3.1.4. The centrality dependence of the slope of $v_1(y)$ around midrapidity* Results from BES Phase-II will greatly strengthen the findings of a non-monotonic variation in the slope of $v_1(y)$ for protons and net-protons. It is proposed to study the centrality dependence of $v_1$ by taking high statistics data with the detector upgrades discussed below. The proposed statistics (see Table 2) at each energy will allow us to measure the centrality dependence of the slope of $v_1$ in a step size of 5% in centrality for protons, antiprotons, and net-protons, each with comparable statistics as achieved in our BES-I analysis, which focused on only a single wide bin (10-40% centrality).

The panel on the left in Fig. 23 reproduces (in red) the BES-I measurement of proton directed flow versus beam energy at intermediate centrality, namely 10–40%. This relatively wide centrality bin shows a statistically significant minimum in mid-rapidity $v_1$ slope between 11.5 and 19.6 GeV. The upper green curve in this panel shows the approximate upper bound of the measured $dv_1/dy$ range for protons in central collisions (0–10%), and the lower green curve shows the approximate lower bound for peripheral collisions (60–80%). These green curves indicate a remarkably strong centrality dependence. With the present BES-I statistics,

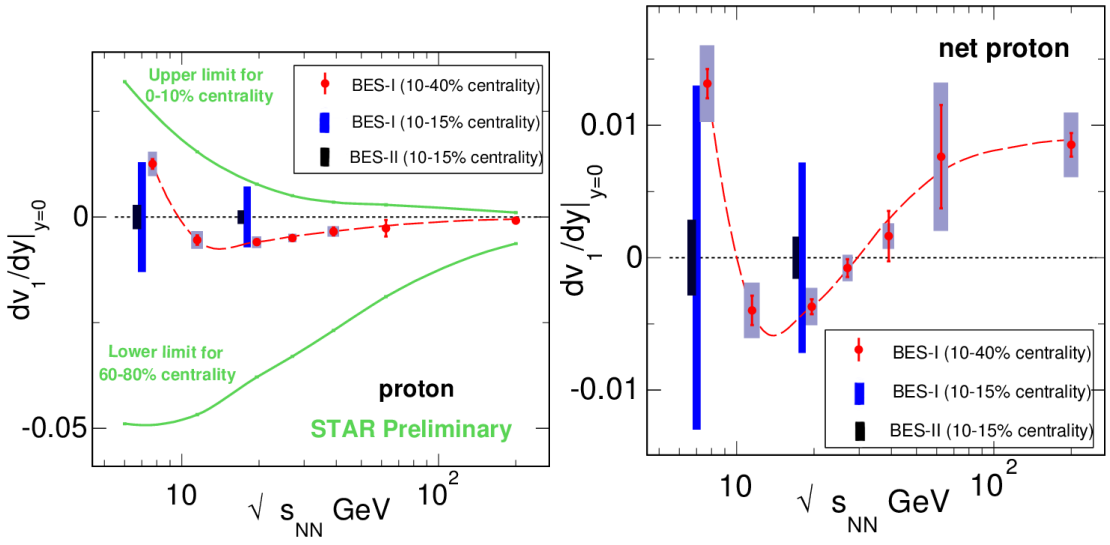


**Figure 23.** Left panel: Statistical errors with narrow centrality bins for proton $dv_1/dy$ near midrapidity at two sample beam energies for BES-I data sets (blue error bars; the points are arbitrarily placed at $dv_1/dy = 0$) and with the proposed BES Phase-II data sets (black error bars). Right panel: The same, but for net-protons.

it is not possible to determine if there is any minimum at all, much less identify where it might lie along the beam-energy axis, for either central or peripheral collisions. With the improved BES Phase-II statistics, this crucial phenomenology can, very likely, be fully mapped-out. Specifically, the blue error bars in Fig. 23 illustrate the statistical uncertainty with the indicated narrow centrality bin based on BES-I measurements, whereas the black error bars are a projection of the expected statistical errors in the same narrow centrality bin with the proposed BES Phase-II measurements. The projections presented in the right-hand panel of Fig. 23 indicate that the centrality dependence of net-proton directed flow will be a feasible measurement for the first time when BES Phase-II data become available.

The relatively small BES-I data sets provide only very limited information about centrality dependence as mentioned above, yet it is already evident (for example, from the left panel of Fig. 23) that the beam energy where the proton $v_1$ slope changes sign (which also is the lowest of the two sign changes in the case of net-protons) is a strong function of centrality. Part of this sensitivity to centrality may be related to the fact that different centrality selections at a given beam energy change the baryon chemical potential. Given that one interpretation of the minimum in proton and net-proton $v_1$ slope associates it with the EOS softest point, there is evidently also a dependence of this same observable on centrality. It is clear that there is a rich and detailed phenomenology associated with the $v_1$ behavior in the vicinity of the minimum, including its centrality dependence, and any model used to interpret these data and to infer properties of the QCD phase diagram in the vicinity of a possible first-order phase transition needs to be confronted by the complete phenomenology of the effect, thereby minimizing the chance of an ambiguous or even incorrect conclusion.

Beyond the greatly improved proton and antiproton directed flow measurements discussed above, BES Phase-II will allow STAR to access $v_1$ for other particle species such as charged and neutral kaons, $\Lambda$, and other hyperons in the region of high baryon density. Measurements of $\Lambda$, $\Xi$ and $K^0_s$ at AGS energies [164], albeit with large statistical errors, have been difficult for the then-available nuclear transport models to explain [49]. BES Phase-II will allow this long-standing challenge for hadronic transport models to be reopened at a slightly higher range of beam energies with greatly improved observational detail.

Extending the $v_1$ measurements in the vicinity of the possible softest point to additional particles species beyond the protons, antiprotons and charged pions already reported by STAR will also bring more richness and detail to the phenomenology. The published $v_1$ measurements show no minimum for produced particles, but a significant minimum apparently associated with transported initial-state baryon number (assuming the hypothesized interpretation). Another way to state the latter point is that up and down flavor originating from the initial colliding nuclei is especially sensitive to the EOS physics under investigation. Baryons like $\Lambda$ at energies around the position of the reported minimum and below have two-thirds of their quarks in common with the proton component of interest, and therefore offer a new way to investigate this hypothesis. As usual, comparisons with all available state-of-the-art models will be essential for any confident conclusion, and it is essential to confront the models with a comprehensive set of measurements.

*3.1.5. Proton-pair correlations* This section outlines one of the promising new analyses planned for BES Phase-II that was not feasible in Phase-I due to insufficient statistics. One of the major goals of the RHIC beam energy scan programs is to find evidence of a first-order phase transition. As the system is only observable at the end of the reaction, we cannot observe directly a discontinuity of one of the state variables (i.e. order parameter). Instead, we rely on the fact that the mixing of phases at the transition causes a softening of the equation of state [165, 166]. Hydrodynamic models predict that there should be a minimum (even a negative value) of the directed flow at the energy which corresponds to the crossing of the phase transition boundary [47, 48, 49, 53]. STAR observed a very compelling and suggestive signal in the proton and net-proton directed flow analysis [54]. But what drives the directed flow? Hydrodynamic expansions drive flow; however, in order to generate a non-zero $v_1$, many models at high energy require emission from a tilted ellipsoid [167, 168, 169, 170]. Theoretical studies suggest that this tilt is established very early, prior to the hydrodynamic expansion [171, 172, 173]. In the Landau framework, there is complete stopping and the emission source would be an ellipsoid with its major axis oriented transverse to the beam axis. In the Bjorken picture, there is complete transparency and the emission source is elongated along the beam axis. Neither picture is correct at the energies spanned by the RHIC BES program. Instead, models are needed to understand the effects of compression and the equation of state. For example, a model using modified string tensions leads to calculations that describe this tilted initial shape [167]. The standard string tension of 1 GeV/fm leads to a Bjorken-style initial shape, while collective effects can be evoked using an effective string tension of 10 GeV/fm and consequently less transparency and an initial tilt to the source [167].

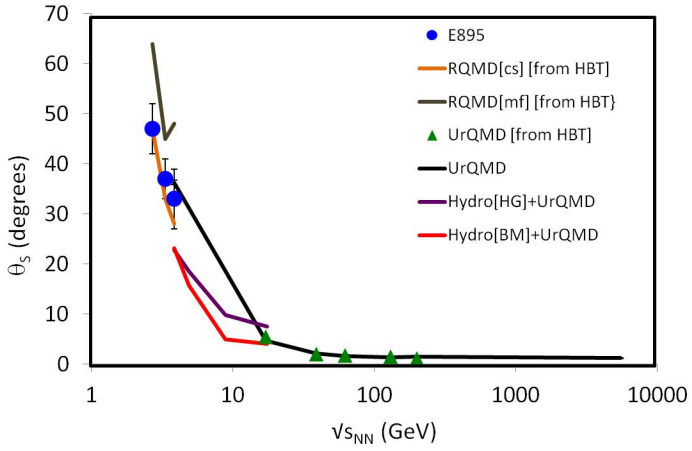


**Figure 24.** The published data on the pion source tilt from 8-33% centrality Au+Au collisions [177] compared to models which include various equation of state prescriptions. These model calculations support the hypothesis that while HBT correlations are still evolving in principle up to the very latest stage of the collision (kinetic freeze-out), they nevertheless offer valuable sensitivity to early-stage physics.

The interesting BES-I results on net-proton $v_1$ and $\kappa\sigma^2$ suggest that one should further explore the correlations among the protons. Studies of azimuthally sensitive pion HBT (asHBT) suggest that experimental measurements of the coordinate-space tilt angle are possible [173, 174, 175]. These asHBT measurements can be used to resolve radii in the outward, sideward, and longitudinal directions ($R_O$, $R_S$, $R_L$, and the cross terms $R_{OL}$, $R_{OS}$, $R_{SL}$). Fourier components of the magnitudes of these radii with respect to the reaction plane can also be developed ($R^2_{S,n} = \langle R_{2S}(\phi)\cos n\phi\rangle$). By appropriately combining the terms, measurements of the eccentricity of the source ($\varepsilon = 2R^2_{S,2}/R^2_{S,0}$) can be extracted; for BES-I, these eccentricity results were submitted for publication [176]. With sufficient signal magnitude and event statistics, the tilt angle, $\theta_S = \frac{1}{2}\tan^{-1}(\frac{-4R^2_{SL,1}}{(R^2_{L,0}-R^2_{S,0}+2R^2_{S,2}}$), can also be extracted. To date, there has been only one experimental measurement of these tilt angles, and this was for two-pion HBT [177]. These results are shown in Fig. 24.

Also shown in Fig. 24 are calculations using RQMD at low energies and UrQMD at higher energies. The straight UrQMD model (black) shows the behavior of a medium that exhibits no phase transition, while the two versions of the model that include a hydro stage of the evolution implicitly contain a phase transition with the properties of the partonic stage being effected by tuning parameters of the model. Note that in this prescription of QCD matter, the presence of a phase transition significantly reduces the tilt angle at a given energy.

There have been preliminary analyses of the source tilt angles using the STAR 10-50% centality BES-I data. From these preliminary tilt angle measurements, we are able to estimate the reduction in the percent error that could be expected with the significant improvement in statistics proposed for BES Phase-II. The estimates for the projected errors for identical-pion asHBT are shown by the red markers on Fig. 25. Note that these are percent errors and that

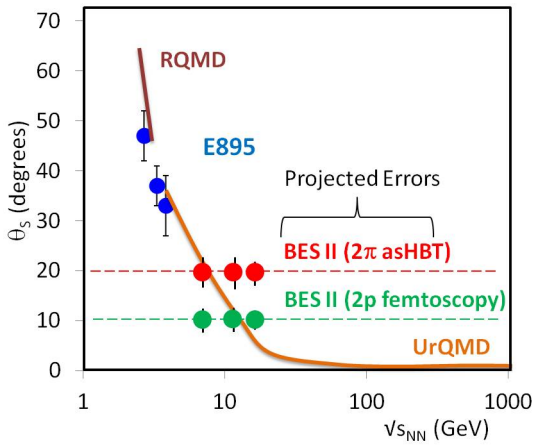


**Figure 25.** Projected errors in $\theta_S$ for BES Phase-II from azimuthally sensitive two-particle correlation analysis of using 10-50% centrality Au+Au collisions as a function of beam energy from two-pion asHBT (red) and two-proton azimuthally sensitive femtoscopy. For comparison lower energy data points are shown for 8-33% centrality Au+Au collisions from two-pion asHBT analysis (blue) [177].

the points are arbitrarily plotted for a 20° tilt angle. Should the angle be smaller, the errors would be correspondingly smaller. As the strongest indication of behavior suggesting a phase transition has been seen in the proton and net-proton directed flow, it will be of even greater interest to study the shape and tilt of the proton emission source. We propose to extend the pion asHBT paradigm [174] to two-proton correlations which has not previously been done. As we have measured the yields of pions and protons at all relevant energies, we can calculate the expected ratio of proton pairs to pion pairs and then appropriately scale the error to make error projections for two-proton azimuthally sensitive femtoscopy in BES Phase-II. These error projections are shown on Fig. 25 in green. Using these error projections, we can also estimate the required statistics for the azimuthally-sensitive measurement for protons at different collision energies and these are listed in Table 2.

*3.1.6. Improved* $\kappa\sigma^2$ *for net-protons* The search for CP location requires quantitative measurements of the variation of of net-proton $\kappa\sigma^2$ with beam energy. The current measurements have large statistical uncertainty at all collision energies from $\sqrt{s_{NN}}$ = 7.7 to 27 GeV. These errors preclude any conclusion of a non-monotonic or monotonic variation of the observable with beam energy. We will need to achieve a statistical error of less than 10% on $\kappa\sigma^2$ for each beam energy in order to determine if the suggestive features of the net-proton higher moments shown in Fig. 5 genuinely establish a non-monotonic behavior which is consistent with a CP.

The estimated statistical errors, for the BES Phase-II energy region $7.7 < \sqrt{s_{NN}} < 19.6$ GeV, for net-proton are shown in Fig. 26 by the green shaded band assuming the required number of events listed in Table 2. The requested high statistics will allow us to pursue the net-proton distribution studies at higher orders (higher than the 4th) where one expects

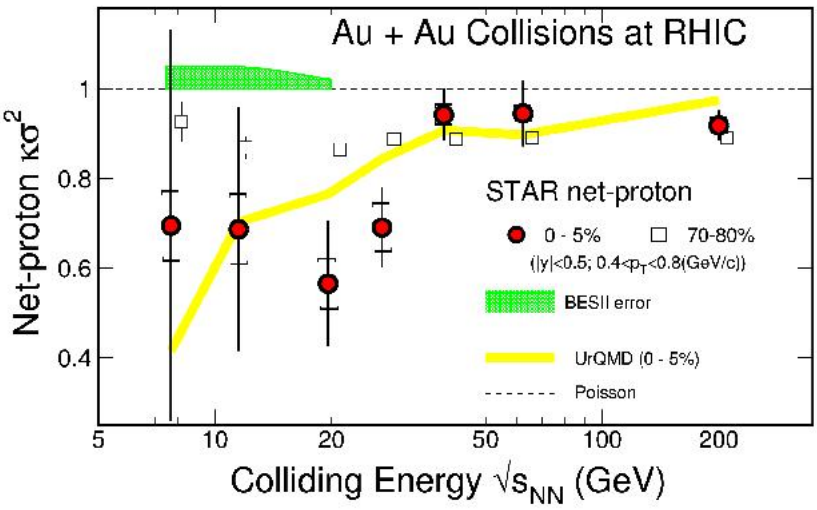


**Figure 26.** Collision energy dependence of net-proton $\kappa\sigma^2$ from central 0-5% (filled-circles) and 70-80% (open-squares) Au+Au collisions at RHIC. The vertical error bars are statistical and the caps correspond to systematic errors. The yellow solid band represents 0-5% central Au+Au collision results from UrQMD simulations. The green shaped band shows the estimated statistical errors for the BES Phase-II, assuming the requested events listed in Table 2.

increased sensitivity to the criticality. In addition, we will also study the higher moments of the net-kaons.

*3.1.7. Dilepton production* With a low material budget and large acceptance, STAR has the unique opportunity to carry out a systematic study of dilepton production in high total-baryon density environments. Having established the capability to do such measurements at higher energies, we propose to extend the same to lower beam energies.

As is illustrated in Fig. 17, we find the LMR excess to be consistent with model predictions that indicate an approaching symmetry restoration, driven by baryon density and temperature. In Fig. 18, it is shown that with decreasing beam energy, the total baryon density, by proxy of $(p+\bar{p})/(\pi^+ + \pi^-)$, remains fairly constant from top RHIC down to top SPS center-of-mass energies, while increasing with further decreasing beam energies. As is indicated in Fig. 27, the expectation is that the LMR excess will increase by a factor of 2. This is within STAR's BES Phase-II sensitivity and will be the last piece of strong evidence for chiral symmetry restoration, implemented in models which describe all the dilepton data, so far. At the same time, measurements of the IMR would allow us to determine how this range may smoothly transition and match to the $p_T$ slopes in the LMR. While the charm contribution in the LMR range will significantly drop with lower beam energies, these rates continue to dominate the IMR. During BES Phase-II the improved muon detection capabilities, thanks to

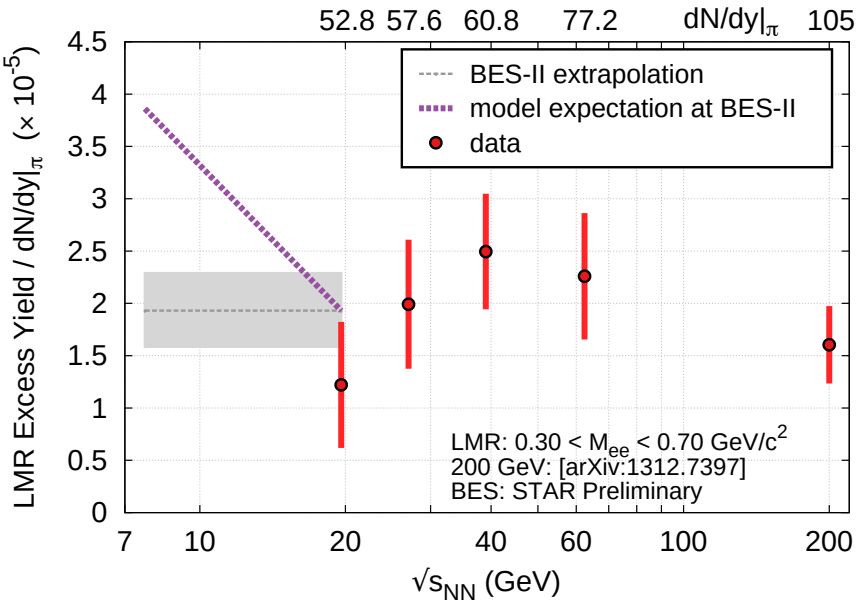


**Figure 27.** This plot summarizes our current measurements. The data points are the integral LMR excess (data-cocktail) between 300 and 700 MeV/$c^2$ normalized the measured $\pi$ multiplicity for BES minimum-bias events. The grey dotted line below 20 GeV indicates the average normalized excess, while the grey band indicates the projected uncertainty in the proposed BES Phase-II measurements. The purple dotted line shows the expected increase by a factor of two in normalized excess yield as the beam energy is further lowered to 7 GeV.

the 2014 MTD upgrade, will allow for independent measurements, through $e-\mu$ correlations, of the charm contribution to the dilepton continuum. In addition, with its trigger capabilities, the MTD will allow to efficiently trigger on the dimuon channel, which suffers significantly less from the large backgrounds that complicate dielectron measurements.

The requirement in the LMR is to achieve a similar level of statistical uncertainty as is reached for STAR's $\sqrt{s_{NN}}$ =200 GeV dielectron data sample. Based on the BES-I 19.6 GeV data sample of less than 40M events, this would imply about 400M minimum-bias events at that particular energy. As the signal-to-background ratio is expected to improve for the lower energies due to a significant reduction in the contributions from the combinatorial background and the $c\bar{c}$ continuum, the required event samples are reduced by factors of up to $\sim 4$ for the lowest energies. The improvement needed in the IMR is estimated based on the statistical uncertainties of the dielectron mass slope from the same BES-I data set at $\sqrt{s_{NN}} = 19.6$ GeV. A factor of 10 more (minimum-bias) events would bring that uncertainty to about 10%. Note that this is comparable to the requested improvement in statistics for the LMR measurements.

### *3.2. Beam request*

The previous section details the precision with which each observable must be measured in order to draw conclusions which quantitatively answer the four key questions. Each of these questions places different demands on the experimental program.

The first goal of the BES program, namely the evidence for the disappearance of signatures of quark-gluon phase observed at the RHIC top energy, is already qualitatively reached with the results of BES-I. Needless to say, that the enlarged statistics of BES Phase-II would allow us to improve on accuracy of earlier results, and to precisely determine at which collision energy QGP signatures disappear thus establishing the onset of deconfinement. The QGP signatures all seem to disappear at the low end of the BES-I energy range, which is consistent with the prior claim of the onset of deconfinement at 7.7 GeV [13, 178]. In order to test this claim and to establish precisely the energy of the onset of deconfinement it will be necessary to make measurements at energies around and below 7.7 GeV. A collision energy at 6.4 GeV would be optimal, however the collider performance is dropping rapidly for these lowest energies (see section 3.5), therefore we are exploring the possiblity of using an internal fixed-target to allow us to access collision energies below 7.7 GeV. This option is discussed in section 3.3.

Note, that the second and third goal, the discovery of first-order phase transition and CP, are equivalent to a large degree. That means that the discovery of one would signal the presence of the other. The net-proton $v_1$ measurements seem to imply that the softest point might be at an energy between 11.5 and 19.6 GeV. Clearly, final results from the recent 14.5 GeV dataset will help to clarify the critical energy range to establish a first-order phase transition. The evidence for a critical behavior from the net-proton kurtosis suggests that 19.6 GeV may be the most important energy. Again the recent 14.5 GeV run will help localize the energies of highest interest. The search for the critical point raises the key question of what is the necessary step size in $\mu_B$. We have developed a proposal which uses a step size of 50-60 MeV in $\mu_B$. To establish conclusively the discovery of the CP, it may prove necessary to bracket the key energy with energies corresponding to a finer step size in $\mu_B$. This decision can only be made after the high statisitcs data from the first year (2018) of BES Phase-II are available.

The experimental program proposed will locate CP point if it lies within the search range in $\mu_B$ = 20-420 MeV. If, however, the CP location is at a $\mu_B$ value larger than the $\mu_B$ = 420 MeV which is a maximum $\mu_B$ value accessible with RHIC machine running in colliding mode in 2018/2019, we will continue the search with events obtained in fixed-target mode (see Section 3.3) taken concurrently with the colliding beams operation. This extended $\mu_B$ range will reach to about 720 MeV, which is higher than theoretical predictions presently available call for. Therefore, the present plan for the BES Phase-II covers the chemical potential range from the smallest values of about 20 MeV at RHIC top energies to those high enough to reach and exceed the theoretical expectations. This allows us to bracket the location of the Critical Point from both sides.

Finally, it is important to push the study of chiral symmetry restoration through dilepton

**Table 3.** Beam Energy Scan Phase-II proposal for 22 weeks of RHIC running in each of the years 2018 and 2019.

| Collision Energy (GeV) | 7.7 | 9.1 | 11.5 | 14.5 | 19.6 |
|---|---|---|---|---|---|
| $\mu_B$ (MeV) in 0-5% Central Collisions | 420 | 370 | 315 | 260 | 205 |
| BES-I (Million Events) | 4 | – | 12 | 20 | 36 |
| BES-I Event Rate (Million Events/Day) | 0.25 | 0.6 | 1.7 | 2.4 | 4.5 |
| BES-I Int. Luminosity ($1\times10^{25}$/cm$^2$ s) | 0.13 | 0.5 | 1.5 | 2.1 | 4.0 |
| e-Cooling Luminosity Improvement Factor | 4 | 4 | 4 | 8 | 15(4) |
| BES Phase-II (Million Events) | 100 | 160 | 230 | 300 | 400 |
| Required Beam Time (Weeks) | 14 | 9.5 | 5.0 | 2.5 | 4.0+ |

measurements down to the region of the expected highest baryon density, which would be a collision energy of about 8 GeV.

The above paragraph outlines our best understanding of the most important energy ranges and the necessary energy step sizes. The previous Section (3.1) detailed the required statistics for the key measurements at each proposed energy. It is assumed that there will be 22 cryo-weeks of RHIC running in each of the years 2018 and 2019. Based on these goals, requirements, constraints, and assumptions, we have developed a proposal for the BES Phase-II which is summarized in Table 3. The proposed number of weeks of RHIC running at 7.7 GeV has been estimated by considering the corresponding average event rate in the final week of BES-I operations, BES-I luminosity, an electron cooling luminosity improvement factor mid-way between the optimistic and pessimistic estimates (see Section 3.5), and the number of events required for the physics program as per Table 2. The proposed number of weeks for beam energies of 11.5 and 19.6 GeV are obtained using the average numbers for event rate and luminosity over the entire collider running period, and the event statistics as desired in BES Phase-II (Table 2). There is an additional uncertainty on the rate estimates for the 19.6 GeV system, and that arises because without an improvement to the trigger, the raw data rate will exceed the limits of the STAR DAQ system. The situation should be significantly improved with the help of the cleaner beam after electron cooling, and with the help of the Event Plane Detector (EPD) upgrade described in Section 3.6. The numbers of weeks proposed for RHIC running at 9.1 and 14.5 GeV are estimated by interpolating the required numbers between the adjacent energy points.

The sum of the requests over all beam energies is 35 weeks. Adding one week of setup for each energy, and allowing two weeks of cool-down (warm-up) at the start (end) of each year, brings the grand total to 44 weeks. The approach outlined in Table 3 is the optimal strategy based on the information available at this time. However, we acknowledge that there will also be lessons learned from the final analysis of the 14.5 GeV run and from analyses of the first year of the BES Phase-II program. These new data may cause us to re-visit the strategies and priorities of the program. The presented BES Phase-II program, outlined in Table 3, is very strong. Thanks to analysis of the BES-I data, we were able to establish a clear path to discovery and a to establish the magnitude of statistics needed to provide evidence for the physics discussed in all of our program goals.

### *3.3. The Fixed-Target Program*

Several observables show intriguing threshold behavior at roughly $\sqrt{s_{NN}}$ = 7.7 GeV, see Fig. 7 and Ref. [13]. These observations have been used to suggest that this energy corresponds to the onset of deconfinement [13, 178]. In order to test this conjecture, the RHIC BES Phase-II program needs to go to energies below 7.7 GeV. These lowest energies have proven to be challenging for the collider (see Section 3.5). However, it has been demonstrated that with the addition of a stationary gold target placed inside the beampipe, energies of $\sqrt{s_{NN}}$ = 3.0, 3.2, 3.5, 3.9, and 4.5 GeV could be studied. These energies correspond to collisions between gold projectiles tuned for collisions at 7.7, 9.1, 11.5, 14.5, and 19.6 GeV respectively and the stationary gold fixed-target. The proof of principle was already successfully tested in run 14 during the 14.5 GeV Au+Au program. The stationary gold target was mounted at the entry to the TPC as shown in Fig. 28. Preliminary data show that the fixed-target trigger was properly selecting fixed-target events and rejecting beam-beam collisions. An example of event reconstruction of Au+Au at $\sqrt{s_{NN}}$= 3.9 GeV is shown in Fig. 29. It will be important to cross-check the results of the fixed-target program with those of the collider program. By tuning the collider for 62.4 GeV collisions, it will be possible to take a fixed-target dataset at $\sqrt{s_{NN}}$ = 7.7 GeV which can be compared to the 7.7 GeV collider data. The primary physics goals of this part of the program will focus on observables which are sensitive to a softening of the equation of state, as it is expected that the first entry into the mixed-phase will occur at energies below the onset of deconfinement [165, 179, 180].

### *3.4. The Importance of p+p and p+A Systems*

In order to understand fully heavy-ion collisions at a given collision energy, and particularly to understand the partonic stage, it is important to measure $p$+$p$ and $p$+A collisions which will provide the proper reference to allow the effects of the initial states to be identified, measured, and separated from those which are due to the partonic medium, which is assumed to be formed only in heavy-ion collisions. Therefore, the ideal BES Phase-II would have a companion $p$+$p$ and $p$+A scan program which would cover the same collision energies. Collisions of $p$+$p$ are also essential for dielectron measurements, to demonstrate cocktail accuracy as a baseline for Au+Au. These measurements are so far missing in the BES energy region and, if present, they would significantly reduce cocktail uncertainties and help in the extrapolation of yields from SPS to top RHIC energies. At RHIC, the higher charge-to-mass ratio of the proton with respect to gold nuclei allows only for $p$+$p$ and $p$+A collisions at energies of 19.6 GeV and above, letting us study the upper limit of energy span of BES Phase-II with $p$+$p$ and $p$+Au collisions, but missing the main energy region (below 19.6 GeV). Even so, studying $p$+$p$ and $p$+A collisions at 19.6 GeV indeed might prove to be extremely important. For the rest of the BES Phase-II energy range, we will resort to using peripheral collisions as our proxy for the $p$+$p$ reference data. It should be noted that peripheral collisions are not an alternative option for the dilepton measurements.

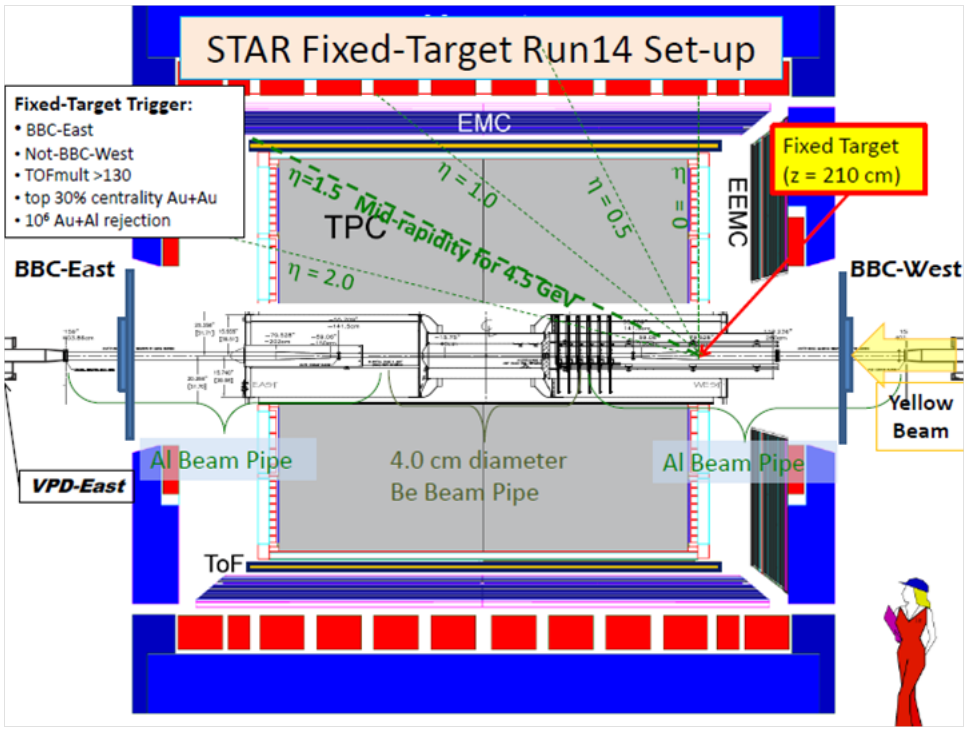


**Figure 28.** A Schematic diagram of STAR showing the fixed-target location for the tests in 2014. The target is a 1mm think gold foil; the projectiles are ions from the halo of the yellow beam.

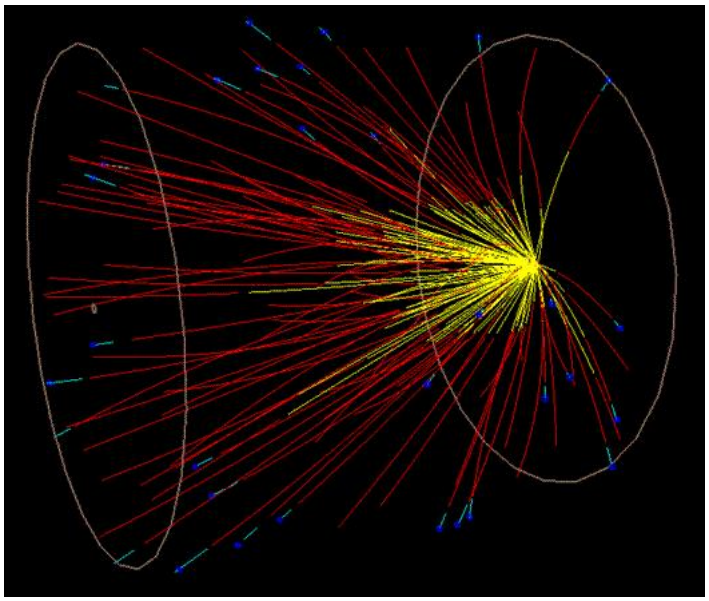

**Figure 29.** The reconstructed tracks from an interaction between a nucleus in the beam halo and a gold nucleus in the stationary target positioned at the entrance to the TPC ($z$ = 210 cm). This is a central event at $\sqrt{s_{NN}}$ = 3.9 GeV (Au beam with $E_{Total}$ of 7.25 GeV on stationary target). The detector has good acceptance from target rapidity to 0.4 units forward of mid-rapidity.

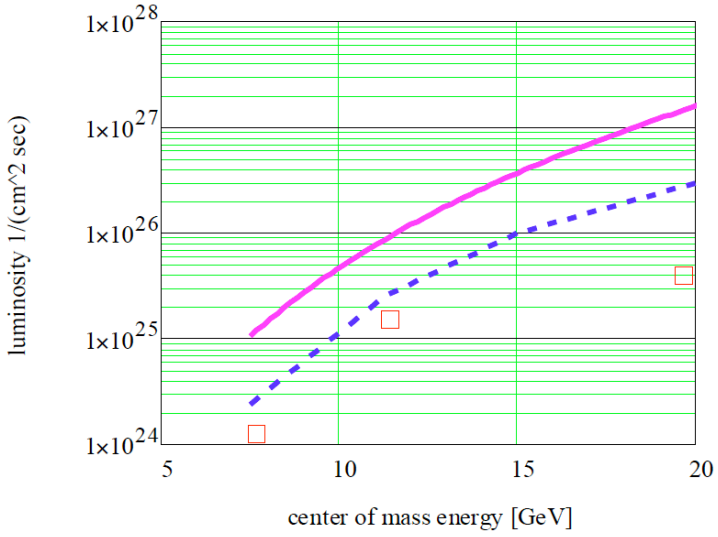


**Figure 30.** Projection of averaged store luminosity within ±1 m vertex for Au ions in RHIC. The lines represent the optimistic (red) and pessimistic (blue) estimates for the luminosity which will be achieved with electron cooling. The open squares are the luminosities reached in BES-I.

### *3.5. Collider Performance*

As discussed above, the major thrust of the BES Phase-II program is to make high statistics measurements of the observables presented in this document for Au+Au collisions at $\sqrt{s_{NN}} <$ 20 GeV. This requires the operation of RHIC with luminosities significantly increased over those which were achieved during BES-I. This will be accomplished by constructing an electron cooling system to reduce the transverse beam emittance and by developing the ability to stretch the bunches longitudinally to reduce the intra-beam Coulomb scattering.

The original design of RHIC optimized the luminosity at $\sqrt{s_{NN}}$ = 200 GeV. At lower energies, the beam is not as well-focused and the collision rate is low. In order to provide adequate intensity for BES Phase-II, the RHIC Collider Accelerator Division has been undertaking,as mentioned above, an upgrade with electron cooling (Fig. 30). According to simulations, with the proposed electron superconducting RF gun, the luminosity will increase by a factor of 2-5 at $\sqrt{s_{NN}}$ = 7.7 GeV and by a factor of 8-20 at $\sqrt{s_{NN}}$= 20 GeV. Additional luminosity increases will be made possible by stretching the beam bunches beyond the usual 6 ns length.

All of these advances make it possible to achieve the event statistics required for the key measurements listed in Table 2.

### *3.6. Detector Upgrades*

The following aspects of BES Phase-II physics program will benefit from presently planned improvements and upgrades to the various sub-systems of the STAR detector.

- **Better acceptance for the STAR TPC in rapidity and $p_T$:** (i) This will enable the study of rapidity dependence of freeze-out dynamics. For a given beam energy, expanding the rapidity range offers the possibility of extending the $\mu_B$ range, thereby scanning a larger part of the phase diagram. (ii) It will extend measurements of $v_1$ beyond the information contained in the slope of $v_1(y)$ close to midrapdity. A broadened rapidity acceptance will expand our understanding of the role of baryon transport on the $v_1$ measurements. (iii) It will permit us to study of the rapidity dependence of higher moments of net-proton/net-charge distributions, to understand the role of charge/baryon number conservation, to provide an experimental approach to determine the effect phase-space limitations on the critical fluctuations measurements, and reduce the effect of centrality resolution on the higher moments [43]. (iv) It will improve the low $p_T$ acceptance, which will better constrain the physics of freeze-out dynamics, by reducing the systematic uncertainties associated with extracting the yields of various particles. (v) It will improve the strange and multi-strange hadron reconstruction efficiency, which will strengthen quantitative conclusions about partonic collectivity.
- **Centrality determination:** Currently, STAR uses the charged particle multiplicity measured in the TPC to determine the collision centrality. Fluctuation and correlation measurements are particularly sensitive to possible correlations between the charged tracks used for physics analysis and those used for centrality determination. This is best avoided, and will be achieved if collision centrality is determined from a separate detector in a different pseudorapidity region from the TPC.
- **Event-plane determination:** Measurements of elliptic flow in BES-I used the TPC for the event plane determination. Non-flow effects have been reduced by keeping an $\eta$ gap (currently $\sim 0.1$– $0.2$) between the particles used for the correlation measurement and the event plane measurement. A dedicated event-plane detector centered at a pseudorapidity of 3 units would result in an $\eta$ gap of about 2 units of pseudorapidity and thus would decrease the non-flow effects. Directed flow measurements in BES-I used the BBC detectors, which have poor event-plane resolution. A dedicated event-plane detector would improve physics performance and facilitate physics interpretation in such analyses also.
- **Trigger performance:** The transverse beam size at the lowest RHIC energies was significantly greater than at $\sqrt{s_{NN}} = 200$ GeV, causing collisions of ions in the beam halo with either the beam pipe or support-structure materials. At $\sqrt{s_{NN}} = 7.7$ GeV, 80–98% of the triggered reactions came from such beam on beam-pipe collisions. The situation will improve with the installation of an electron gun. A total increase in luminosity of about a factor 10 is expected, which will result in a trigger rate of several kHz at the highest BES energy. To exploit this, it is essential to trigger on all good Au+Au collisions with a reconstructible vertex.

*3.6.1. iTPC* It is proposed [181] to upgrade the inner sectors of the STAR TPC to increase the segmentation on the inner pad plane and to renew the inner-sector wires, which are

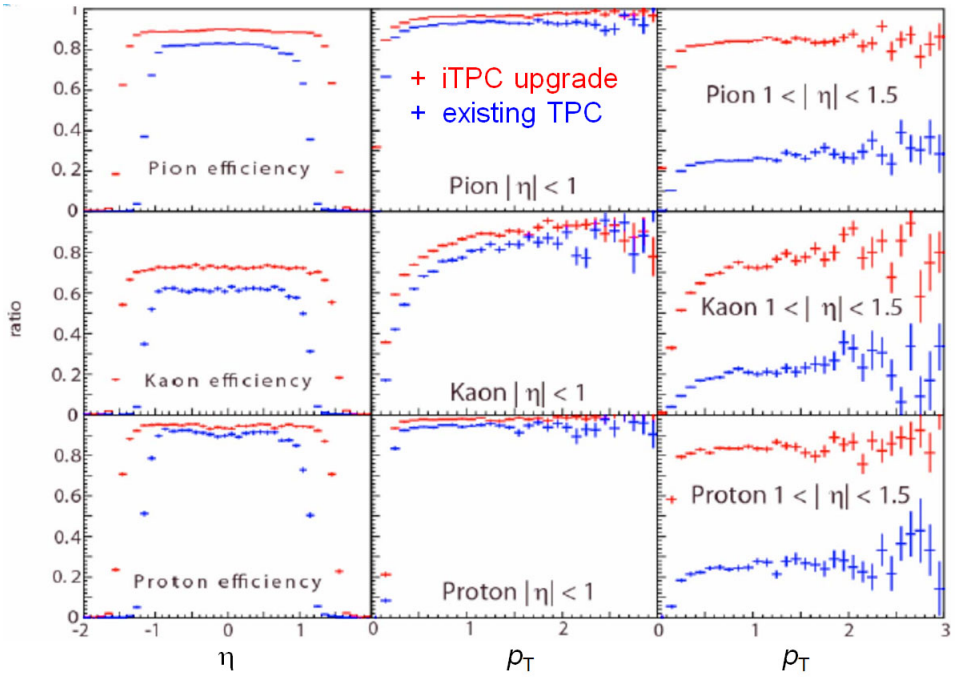


**Figure 31.** Pseudorapidity and transverse momentum dependence of the detection efficiencies for pions (top panel), kaons (middle panel), and protons (bottom panel). Blue and red points are the results for TPC and iTPC, respectively [181].

showing signs of aging. The upgrade will provide better momentum resolution, better $dE/dx$ resolution, improved acceptance at high rapidity to $|\eta| < 1.7$ compared to the current TPC configuration of $|\eta| < 1.0$, and higher track reconstruction efficiency. Figure 31 shows the improved acceptance in $p_T$ and $y$ for reconstructed pions, kaons and protons. Although iTPC will allow significantly improved tracking and coverage out to $|\eta| < 1.7$, the longitudinal boost for higher rapidity particles shifts the low $p_T$ particles into a momentum range where it becomes increasingly challenging to employ PID through relative ionization in the TPC. The PID capabilites will be supplemented with the inclusion of one prototype sector of the End-Cap Time-of-Flight (eTOF) [182]. Although the eTOF prototype will only have a narrow azimuthal acceptance, this will enable key inclusive measurements. The enhanced performance made possible by the iTPC will not only benefit the BES Phase-II physics program but will also be crucial for STAR's future program with $p$+$p$/$p$+A and $ep/e$A collisions at forward higher-rapidity regions.

*3.6.2. EPD* The EPD [183] is a dedicated event-plane and centrality detector placed in the forward rapidity region $2 < |\eta| < 4$. With segmentations in both radial and azimuthal directions, the detector will provide precise measurements of both the collision centrality and the event plane. As shown in Fig. 32, the proposed EPD configurations with 12 or 30 $\phi$-segmentations are both very close to the optimal case. Additionally, the EPD will be a good trigger detector for collisions at lower beam energies.

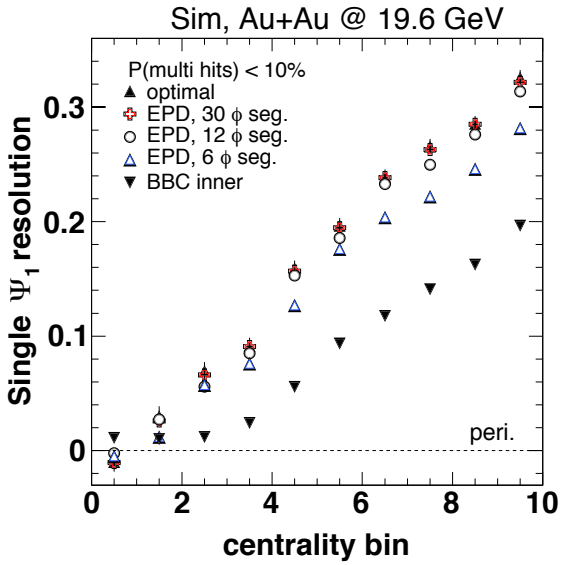


**Figure 32.** First-harmonic event-plane resolution as a function of collision centrality for different detector segmentations [183].

## 4. Summary

The data from BES-I have allowed significant progress to be made toward the goals that had been established at the outset of this program. There is a clear indication that hadronic interactions dominate at the lower BES energies and several observables associated with the formation of a partonic phase at top RHIC energy have been turned-off. These findings corroborate the establishment of QGP at the top RHIC energy. The BES-I program, with limited event statistics, has made important measurements towards critical point and first-order phase transition physics. This provides compelling reasons for high event statistics in a second phase of the program. These results from the BES-I have allowed us to focus the proposed BES Phase-II on the most crucial energy range from 7.7 to 20 GeV. Using the results from the BES-I program, we have been able to make estimates of the projected errors in a future program and using these we have been able to determine the statistics required for each observable in order to allow us to draw firm conclusions. The enhanced collider performance via increased luminosity due to electron cooling and longer bunches will allow for higher-precision measurements of the key observables. Furthermore, STAR detector upgrades (iTPC and EPD) will allow more comprehensive and refined measurements. A set of focused, high-precision, refined measurements will allow the BES Phase-II program to fundamentally enhance our understanding of the phase diagram of QCD matter.

**Acknowledgements**

We would like to thank Drs. Francesco Becattini, Elena Bratkovskaya, Alexei Fedotov, Sourendu Gupta, Frithjof Karsch, Cheming Ko, Volker Koch, Olena Linnyk, Jinfeng Liao, Christoph Montag, Hannah Petersen, Owe Phillpsen, Krishna Rajagopal, Ralf Rapp, Jan Steinheimer, Misha Stephanov, Swagato Mukherjee, Ivan Vitev for their invaluable contributions to this document. We thank the RHIC Operations Group and RCF at BNL, the NERSC Center at LBNL, the KISTI Center in Korea, and the Open Science Grid consortium for providing resources and support. This work was supported in part by the Offices of NP and HEP within the U.S. DOE Office of Science, the U.S. NSF, CNRS/IN2P3, FAPESP CNPq of Brazil, the Ministry of Education and Science of the Russian Federation, NNSFC, CAS, MoST and MoE of China, the Korean Research Foundation, GA and MSMT of the Czech Republic, FIAS of Germany, DAE, DST, and CSIR of India, the National Science Centre of Poland, National Research Foundation (NRF-2012004024), the Ministry of Science, Education and Sports of the Republic of Croatia, and RosAtom of Russia.

**References**

[1] E. Laermann and O. Philipsen, Ann. Rev. Nucl. Part. Sci. **53** (2003) 163.
[2] K. Fukushima and T. Hatsuda, Rept. Prog. Phys. **74** (2011) 014001.
[3] J. C. Collins and M. J. Perry, Phys. Rev. Lett. **34** (1975) 1353.
[4] E. V. Shuryak, Phys. Rept. **61** (1980) 71.
[5] Y. Aoki, Z. Fodor, S. D. Katz and K. K. Szabo, Phys. Lett. B **643** (2006) 46.
[6] Y. Aoki, S. Borsanyi, S. Durr, Z. Fodor, S. D. Katz, S. Krieg and K. K. Szabo, JHEP **0906** (2009) 088.
[7] S. Borsanyi *et al.*, [Wuppertal-Budapest Collaboration], JHEP **1009** (2010) 073.
[8] A. Bazavov *et al.*, Phys. Rev. D **85** (2012) 054503.
[9] Y. Aoki, G. Endrodi, Z. Fodor, S. D. Katz and K. K. Szabo, Nature, **443** (2006) 675.
[10] S. Ejiri, Phys. Rev. D **78** (2008) 074507.
[11] E. S. Bowman and J. I. Kapusta, Phys. Rev. C **79** (2009) 015202.
[12] M. A. Stephanov, Prog. Theor. Phys. Suppl. **153** (2004) 139; Int. J. Mod. Phys. A **20** (2005) 4387.
[13] C. Alt *et al.*, [NA49 Collaboration], Phys. Rev. C **77** (2008) 024903.
[14] B. I. Abelev *et al.*, [STAR Collaboration], STAR Internal Note - SN0493, 2009.
[15] B. I. Abelev *et al.*, [STAR Collaboration], Phys. Rev. C **81** (2010) 024911.
[16] P. Braun-Munzinger and J. Stachel, Nature, **448** (2007) 302.
[17] B. I. Abelev *et al.*, [STAR Collaboration], Phys. Rev. C **79** (2009) 034909.
[18] S. Wheaton and J. Cleymans, Comput. Phys. Commun. **180** (2009) 84.
[19] J. Cleymans, H. Oeschler, K. Redlich and S. Wheaton, Phys. Rev. C **73** (2006) 034905.
[20] A. Andronic *et al.*, Nucl. Phys. A**834**, (2010) 237.
[21] A. Andronic, P. Braun-Munzinger and J. Stachel, Nucl. Phys. A **772** (2006) 167.
[22] L. Kumar, [STAR Collaboration], Nucl. Phys. A **904, 905** (2013), 256c.
[23] S. Das, [STAR Collaboration], arXiv:1402.0255.
[24] F. Becattini, *et al.*, Phys. Rev. Lett. **111** (2013) 082302.
[25] S. Chatterjee, R. M. Godbole and S. Gupta, Phys. Lett. B **727** (2013) 554.
[26] S. Borsanyi, *et al.*, Phys. Rev. Lett. **111** (2013) 062005.
[27] A. Bazavov, *et al.*, Phys. Rev. Lett. **109** (2012) 192302.
[28] R. V. Gavai and S. Gupta, Phys. Lett. B **696** (2011) 459.
[29] S. Gupta, X. Luo, B. Mohanty, H. G. Ritter and N. Xu, Science, **332** (2011) 1525.
[30] S. Datta, R. V. Gavai and S. Gupta, Nucl. Phys. A **904-905** (2013) 883c.

[31] Z. Fodor and S. D. Katz, JHEP **0404** (2004) 050.
[32] E. Schnedermann, J. Sollfrank and U. W. Heinz, Phys. Rev. C **48** (1993) 2462.
[33] B. Abelev *et al.*, [ALICE Collaboration], Phys. Rev. C **88** (2013) 044910.
[34] J. Adams *et al.* [STAR Collaboration], Nucl. Phys. A **757**, 102 (2005).
[35] M. A. Stephanov, Phys. Rev. Lett. **102**, 032301 (2009).
[36] M. A. Stephanov, Phys. Rev. Lett. **107**, 052301 (2011).
[37] M. Asakawa, S. Ejiri and M. Kitazawa, Phys. Rev. Lett. **103**, 262301 (2009).
[38] M. Cheng *et al.*, Phys. Rev. D **79**, 074505 (2009).
[39] M. M. Aggarwal, *et al.* , [STAR Collaboration], Phys. Rev. Lett. **105** (2010) 022302
[40] L. Adamczyk, *et al.*, [STAR Collaboration], Phys. Rev. Lett. **112** (2014) 032302.
[41] P. Garg, *et al.*, Phys. Lett. B **726** (2013) 691.
[42] L. Adamczyk, *et al.*, [STAR Collaboration], arXiv:1402.1558.
[43] X. Luo, J. Xu, B. Mohanty and N. Xu, J. Phys. G **40** (2013) 105104.
[44] S. A. Bass, *et al.*, Prog. Part. Nucl. Phys. **41** (1998) 255.
[45] M. Bleicher, *et al.*, J. Phys. G **25** (1999) 1859.
[46] B. Schaefer and J. Wambach, Phys.Rev. D **75** (2007) 085015.
[47] D. H. Rischke, Y. Pursun, J. A. Maruhn, H. Stöcker and W. Greiner, Heavy Ion Phys. **1** (1995) 309.
[48] J. Brachmann, *et al.*, Phys. Rev. C **61** (2000) 024909.
[49] H. Stöcker, Nucl. Phys. A **750** (2005) 121.
[50] A. M. Poskanzer and S. A. Voloshin, Phys. Rev. C **58** (1998) 1671.
[51] L. Van Hove, Phys. Lett. B **118** (1982) 138.
[52] H. Petersen, J. Steinheimer, G. Burau, M. Bleicher and H. Stöcker, Phys. Rev. C **78** (2008) 044901.
[53] J. Steinheimer, J. Auvinen, H. Petersen, M. Bleicher and H. Stöcker, arXiv:1402.7236.
[54] L. Adamczyk, *et al.*, [STAR Collaboration], Phys. Rev. Lett. **112** (2014) 162301.
[55] V. P. Konchakovski, W. Cassing, Y. B. Ivanov, and V. D. Toneev, arXiv:1404.2765.
[56] M. Isse, A. Ohnishi, N. Otuka, P. K. Sahu and Y. Nara, Phys. Rev. C **72** (2005) 064908.
[57] L. Ahle, *et al.*, [E866 and E917 Collaborations], Phys. Lett. B **476** (2000) 1.
[58] L. Ahle, *et al.*, [E866 and E917 Collaborations], Phys. Lett. B **490** (2000) 53.
[59] L. Ahle, *et al.*, [E802 Collaboration], Phys. Rev. C **57** (1998) 466.
[60] L. Ahle, *et al.*, [E-802 and E-866 Collaborations], Phys. Rev. C **60** (1999) 044904
[61] J. L. Klay, *et al.*, [E895 Collaboration], Phys. Rev. Lett. **88** (2002) 102301.
[62] J. Barrette, *et al.*, [E877 Collaboration], Phys. Rev. C **62** (2000) 024901.
[63] S. V. Afanasiev, *et al.*, [NA49 Collaboration], Phys. Rev. C **66** (2002) 054902.
[64] E. O'Brien, [PHENIX Collaboration], Nucl. Phys. A **904, 905**, (2013) 264c.
[65] K. Adcox, *et al.*, [PHENIX Collaboration], Nucl. Phys. A **757**, 184 (2005).
[66] M. Gyulassy and L. McLerran, Nucl. Phys. A **750**, 30 (2005).
[67] K. H. Ackermann, *et al.*, [STAR Collaboration], Phys. Rev. Lett. **86** (2001) 402.
[68] C. Adler, *et al.*, [STAR Collaboration], Phys. Rev. Lett. **87** (2001) 182301.
[69] J. Adams, *et al.*, [STAR Collaboration], Phys. Rev. Lett. **92** (2004) 052302.
[70] S. S. Adler, *et al.*, [PHENIX Collaboration], Phys. Rev. Lett. **91** (2003) 182301.
[71] J. Adams, *et al.*, [STAR Collaboration], Phys. Rev. Lett. **91** (2003) 172302.
[72] J. Adams *et al.*, [STAR Collaboration], Phys. Rev. Lett. **91** (2003) 072304.
[73] K. Adcox *et al.*, [PHENIX Collaboration], Phys. Rev. Lett. **88** (2002) 022301.
[74] S. S. Adler *et al.*, [PHENIX Collaboration], Phys. Rev. Lett. **91** (2003) 072301.
[75] B. I. Abelev *et al.*, [STAR Collaboration], Phys. Rev. Lett. **103** (2009) 251601.
[76] B. I. Abelev *et al.*, [STAR Collaboration], Phys. Rev. C **81** (2010) 054908.
[77] B. B. Back *et al.*, [PHOBOS Collaboration], Phys. Rev. C **72** (2005) 051901
[78] B. B. Back *et al.*, [PHOBOS Collaboration], Phys. Rev. Lett. **94** (2005) 122303
[79] J. Adams *et al.*, [STAR Collaboration], Phys. Rev. Lett. **93** (2004) 252301.
[80] S. S. Adler *et al.* , [PHENIX Collaboration], Phys. Rev. Lett. **94** (2005) 232302.
[81] B. I. Abelev *et al.*, [STAR Collaboration], Phys. Rev. Lett. **99** (2007) 112301.

[82] S. K. Tiwari, P. K. Srivastava and C. P. Singh, Phys. Rev. C **85** (2012) 014908.
[83] L. Adamczyk *et al.*, [STAR Collaboration], Phys. Rev. Lett. **110** (2013) 142301.
[84] L. Adamczyk *et al.*, [STAR Collaboration], Phys. Rev. C **88** (2013) 014902.
[85] Y. Burnier, D. E. Kharzeev, J. Liao and H. -U. Yee, Phys. Rev. Lett. **107** (2011) 052303.
[86] J. Steinheimer, V. Koch and M. Bleicher, Phys. Rev. C **86** (2012) 044903.
[87] J. Xu, T. Song, C. M. Ko and F. Li, Phys. Rev. Lett. **112** (2014) 012301.
[88] J. Xu, L. -W. Chen, C. M. Ko and Z. -W. Lin, Phys. Rev. C **85** (2012) 041901.
[89] C.M. Ko, private communications, December, 2013.
[90] J. C. Dunlop, M. A. Lisa and P. Sorensen, Phys. Rev. C **84** (2011) 044914.
[91] D. Molnar and S. A. Voloshin, Phys. Rev. Lett. **91** (2003) 092301.
[92] V. Greco, C. M. Ko and P. Levai, Phys. Rev. C **68** (2003) 034904.
[93] R. J. Fries, B. Muller, C. Nonaka and S. A. Bass, Phys. Rev. C **68** (2003) 044902.
[94] X. Gong, [PHENIX Collaboration], J. Phys. G: Nucl. Part. Phys. **38**, (2011) 124146.
[95] B. Mohanty and N. Xu, J. Phys. G **36** (2009) 064022.
[96] M. Nasim, B. Mohanty and N. Xu, Phys. Rev. C **87** (2013) 014903.
[97] B. I. Abelev *et al.*, [STAR Collaboration], Phys. Lett. B **673** (2009) 183.
[98] Z. -W. Lin and C. M. Ko, Phys. Rev. C **65** (2002) 034904.
[99] Z. -W. Lin, C. M. Ko, B. -A. Li, B. Zhang and S. Pal, Phys. Rev. C **72** (2005) 064901.
[100] B. B. Back *et al.*, [PHOBOS Collaboration], Phys. Rev. Lett. **91** (2003) 072302.
[101] I. Arsene *et al.*, [BRAHMS Collaboration], Phys. Rev. Lett. **91** (2003) 072305.
[102] X. -N. Wang and M. Gyulassy, Phys. Rev. Lett. **68** (1992) 1480.
[103] I. Vitev and M. Gyulassy, Phys. Rev. Lett. **89** (2002) 252301.
[104] M. Gyulassy, P. Levai and I. Vitev, Phys. Rev. Lett. **85** (2000) 5535.
[105] X. -N. Wang, Phys. Rev. C **70** (2004) 031901.
[106] M.L. Miller, K. Reygers, S. J. Sanders and P. Steinberg, Ann. Rev. Nucl. Part. Sci. **57** (2007) 205.
[107] N. Novitzky, [PHENIX Collaboration], J. Phys. G: Nucl. Part. Phys. **38**, (2011) 124149.
[108] M. Gyulassy and X. -N. Wang, Comput. Phys. Commun. **83** (1994) 307.
[109] B. -W. Zhang, E. Wang and X. -N. Wang, Phys. Rev. Lett. **93** (2004) 072301.
[110] S. Wicks, W. Horowitz, M. Djordjevic and M. Gyulassy, Nucl. Phys. A **783** (2007) 493.
[111] I. Vitev, private communication, (2014).
[112] R. B. Neufeld, I. Vitev and B. -W. Zhang, Phys. Lett. B **704** (2011) 590.
[113] I. Vitev, Phys. Rev. C **75** (2007) 064906.
[114] G. Ovanesyan and I. Vitev, JHEP **1106** (2011) 080.
[115] G. Ovanesyan and I. Vitev, Phys. Lett. B **706** (2012) 371.
[116] P. Huovinen and H. Petersen, Eur. Phys. J. A **48** (2012) 171.
[117] J. Steinheimer and M. Bleicher, Phys. Rev. C **84** (2011) 024905.
[118] C. Nonaka and S. A. Bass, Nucl. Phys. A **774** (2006) 873.
[119] J. Steinheimer, S. Schramm and H. Stocker, Phys. Rev. C **84** (2011) 045208.
[120] D. Kharzeev, R. D. Pisarski and M. H. G. Tytgat, Phys. Rev. Lett. **81** (1998) 512.
[121] D. Kharzeev, Phys. Lett. B **633** (2006) 260.
[122] D. E. Kharzeev, L. D. McLerran and H. J. Warringa, Nucl. Phys. A **803** (2008) 227.
[123] K. Fukushima, D. E. Kharzeev and H. J. Warringa, Phys. Rev. D **78** (2008) 074033.
[124] L. Adamczyk *et al.*, [STAR Collaboration], arXiv:1302.3802.
[125] B. Abelev *et al.*, [ALICE Collaboration], Phys. Rev. Lett. **110** (2013) 012301.
[126] S. A. Voloshin, Phys. Rev. C **70** (2004) 057901.
[127] S. Schlichting and S. Pratt, Phys. Rev. C **83** (2011) 014913.
[128] A. Bzdak, V. Koch and J. Liao, Phys. Rev. C **83** (2011) 014905.
[129] A. Bzdak, V. Koch and J. Liao, Lect. Notes Phys. **871** (2013) 503.
[130] R. Rapp and J. Wambach, Adv. Nucl. Phys. **25** (2000) 1.
[131] J. Alam, S. Sarkar, P. Roy, T. Hatsuda and B. Sinha, Annals Phys. **286** (2001) 159.
[132] G. E. Brown and M. Rho, Phys. Rept. **269** (1996) 333.

[133] D. Adamova *et al.*, [CERES/NA45 Collaboration], Phys. Rev. Lett. **91** (2003) 042301.
[134] R. Arnaldi *et al.*, [NA60 Collaboration], Phys. Rev. Lett. **96** (2006) 162302.
[135] H. van Hees and R. Rapp, Phys. Rev. Lett. **97** (2006) 102301.
[136] J. Ruppert, C. Gale, T. Renk, P. Lichard and J. I. Kapusta, Phys. Rev. Lett. **100** (2008) 162301.
[137] K. Dusling, D. Teaney and I. Zahed, Phys. Rev. C **75** (2007) 024908.
[138] O. Linnyk, E. L. Bratkovskaya, V. Ozvenchuk, W. Cassing and C. M. Ko, Phys. Rev. C **84** (2011) 054917.
[139] A. Adare *et al.*, [PHENIX Collaboration], Phys. Rev. C **81** (2010) 034911.
[140] L. Adamczyk *et al.*, [STAR Collaboration], arXiv:1312.7397.
[141] R. Rapp, Phys. Rev. C **63** (2001) 054907; Phys. Rev. A **83** (2011) 043833.
[142] R. Rapp, J. Wambach and H. van Hees, arXiv:0901.3289.
[143] B. Friman *et al.*, (Eds.), *The CBM Physics Book*, Lect. Notes Phys. 814 [DOI: 10.1007/978-3-462-13293-3]
[144] D. Adamova *et al.*, [CERES/NA45 Collaboration], Phys. Lett. B **666** (2008) 425.
[145] F. Geurts at Rencontres de Moriond QCD 2014, La Thuile, Italy; L. Ruan at QuarkMatter 2014, Darmstadt, Germany.
[146] O. Linnyk, private communication; W. Cassing, E.L. Bratkovskaya, S. Juchem, Nucl. Phys. A **674** (2000) 249.
[147] R. Rapp, Adv. High Energy Phys. **2013** (2013) 148253.
[148] H. van Hees and R. Rapp, Nucl. Phys. A **806** (2008) 339.
[149] D. T. Son and A. R. Zhitnitsky, Phys. Rev. D **70**, 074018 (2004) [hep-ph/0405216].
[150] M. A. Metlitski and A. R. Zhitnitsky, Phys. Rev. D **72**, 045011 (2005) [hep-ph/0505072].
[151] D. E. Kharzeev and D. T. Son, Phys. Rev. Lett. **106** (2011) 062301; arXiv:1208.2537 [hep-ph].
[152] R. Rapp, Phys. Rev. C 63 (2001) 054907
[153] R. Rapp, J. Wambach, H. van Hees, arXiv:0901.3289
[154] J.V. Steele, H. Yamagishi, I. Zahed Phys. Lett. B 384 (1996) 255.
[155] V. Koch, LBNL report 38000, nucl-th/9512029
[156] Y. Burnier, D. Kharzeev, J. Liao and H. Yee, *Phys. Rev. Lett.* **107** (2011) 052303.
[157] M. A. Metlitski and A. R. Zhitnitsky, Phys. Rev. D **72**, 045011 (2005) [hep-ph/0505072].
[158] J. C. Dunlop, M. A. Lisa and P. Sorensen, Phys. Rev. C **84**, 044914 (2011) [arXiv:1107.3078 [hep-ph]].
[159] J. Xu, L. -W. Chen, C. M. Ko and Z. -W. Lin, Phys. Rev. C **85**, 041901 (2012) [arXiv:1201.3391 [nucl-th]].
[160] Gang Wang, Nucl. Phys A **904-905**, 248c (2013).
[161] S.A. Bass *et al* , Prog. Part. Nucl. Phys. **41**, 225 (1998); M. Bleicher *et al* , J. Phys. G: Nucl. Part. Phys. **25**, 1859 (1999).
[162] Y. Burnier, D.E. Kharzeev, J. Liao, H.-U. Yee, arXiv: 1208.2537 (2012); private communication.
[163] Feng Zhao, Quark Matter 2014 conference talk.
[164] P. Chung *et al.* (E895 collaboration), Phys. Rev. Lett. **85** (2000) 940; *ibid* **86** (2001) 2533; *ibid* **91** (2003) 202301.
[165] I. C. Arsene *et al.*, Phys. Rev. C **75** (2007) 034902.
[166] R. Snellings, New J. Phys.13(2011)055008
[167] V. Magas, L.P. Csernai, and D. Strottmann, Nucl. Phys. A **712** (2002) 167.
[168] J. Brachmann *et al.*, Phys. Rev. C **61** (2000) 024909.
[169] L.V.Bravina, Phys. Lett. B **344** (1995) 49.
[170] P. Bozek and I. Wyskiel, Phys. Rev. C **81** (2010) 054902.
[171] H. Sorge, Phys. Rev. Lett. **78** (1997) 2309.
[172] N. Herrmann, J.P. Wessels, and T. Wienold, Annu. Rev. Nucl. Part. Sci. **49** (1999) 581.
[173] G. Graef, M.A. Lisa, M. Bleicher, Phys. Rev. C **89** (2014) 014903.
[174] M. Lisa, U. Heinz, U. Weidemann, Phys. Lett. B **489** (2000) 287.
[175] E. Mount, G. Graef, M. Mitrovski, M. Bleicher, M.A. Lisa, Phys. Rev. C **84** (2011) 014908.
[176] L. Adamczyk *et al.*, [STAR Collaboration], arXiv: 1403.4972; C. Anson, [STAR Collaboration], J. Phys. G: Nucl. Part. Phys. **38** (2011) 124148.
[177] M. Lisa *et al.* (E895 collaboration), Phys. Lett. B **496** (2000) 1.

[178] A. Rustamov, Cent. Eur. J. Phys. **10** (2012) 1267.
[179] J. Randrup, Phys. Rev. C **79** (2009) 054911.
[180] J. Randrup, Phys. Rev. C **82** (2010) 034902.
[181] iTPC upgrade document, (2014):
https://drupal.star.bnl.gov/STAR/upgrade-inner-sectors-time-projection-chamber
[182] eTOF technical document, (2014): https://drupal.star.bnl.gov/STAR/system/files/
[183] EPD technical document, (2014): https://drupal.star.bnl.gov/STAR/system/files/